Biogeosciences
Discussions

Open Access

Implementation of dynamic crop growth processes into a land surface model: evaluation of energy, water and carbon fluxes under corn and soybean rotation

Y. Song[1], A. K. Jain[1], and G. F. McIsaac[2]

[1]Department of Atmospheric Sciences, University of Illinois, Urbana, IL 61801, USA
[2]Department for Natural Resources and Environmental Sciences, University of Illinois, Urbana, IL 61801, USA

Correspondence to: A. K. Jain (jain1@illinois.edu)

BGD
10, 9897–9945, 2013
Implementation of dynamic crop growth processes into a land surface model
Y. Song et al.
Title Page
Abstract / Introduction
Conclusions / References
Tables / Figures
Back / Close
Full Screen / Esc
Printer-friendly Version
Interactive Discussion

Y. Song et al.

Abstract

Worldwide expansion of agriculture is impacting Earth's climate by altering the carbon, water and energy fluxes, but climate in turn is impacting crop production. To study this two-way interaction and its impact on seasonal dynamics of carbon, water and energy fluxes, we implemented dynamic crop growth processes into a land surface model, the Integrated Science Assessment Model (ISAM). In particular, we implement crop specific phenology schemes, which account for light, water, and nutrient stresses while allocating the assimilated carbon to leaf, root, stem and grain pools; dynamic vegetation structure growth, which better simulate the LAI and canopy height; dynamic root distribution processes in the soil layers, which better simulate the root response of soil water uptake and transpiration; and litter fall due to fresh and old dead leaves to better represent the water and energy interception by both stem and brown leaves of the canopy during leaf senescence. Observational data for LAI, above and below ground biomass, and carbon, water and energy fluxes were compiled from two Ameri-Flux sites, Mead, NE and Bondville, IL, to calibrate and evaluate the model performance under corn (C4)-soybean (C3) rotation system over the period 2001–2004. The calibrated model was able to capture the diurnal and seasonal patterns of carbon assimilation, water and energy fluxes under the corn-soybean rotation system at these two sites. Specifically, the calculated GPP, net radiation fluxes at the top of canopy and latent heat fluxes compared well with observations. The largest bias in model results is in sensible heat flux (H) for corn and soybean at both sites. With dynamic carbon allocation and root distribution processes, model simulated GPP and latent heat flux (LH) were in much better agreement with observation data than for the without dynamic case. Modeled latent heat improved by 12–27 % during the growing season at both sites, leading to the improvement in modeled GPP by 13–61 % compared to the without dynamic case.

1 Introduction

Increasing global food demand accelerates deforestation in areas suitable for modern agriculture. Today, croplands and pastures have become the two largest terrestrial biomes, accounting for about 40 % of the planet's land surface (Foley et al., 2005). Additionally, demand for biofuels might exacerbate the expansion of croplands in the coming decades. In 2004, about 1 % of global cropland was being used for biofuels, and this share might increase 3 to 4 times by 2030 (FAO, 2008).

This rapid transformation of landscape can impact the climate by altering the carbon, water and energy fluxes (Sellers, 1992; McGuire et al., 2001; Matthews et al., 2004; Sitch et al., 2005; Brovkin et al., 2006; Bonan, 2008). While climate is affected by the expansion of agriculture land, climate change clearly affects agriculture. Many crops show positive responses to elevated carbon dioxide and low levels of warming, but higher levels of warming often negatively affect growth and yield (Hatfield et al., 2008; Kucharik and Serbin, 2008; Urban et al., 2012).

The overall aim of this study is to evaluate dynamic crop growth processes in a land surface model, the Integrated Science Assessment Model (ISAM) (Jain and Yang, 2009; Yang et al., 2010; El-Masri et al., 2013), to understand and address the interactions between C3/C4 crop growth, seasonal dynamics of carbon, water, and energy fluxes. Our implementation focuses on the corn–soybean rotation, which is the most common crop rotation practice around the world.

A number of land surface models incorporate advanced representations of croplands to better simulate the relationship between crop production, land surface characteristics and the energy and water cycles (Tsvetsinskaya et al., 2001; Kucharik and Brye, 2003; Gervois et al., 2004; Bondeau et al. 2007; Osborne et al., 2007; Lokupitiya et al., 2009; Van den Hoof et al., 2011). Tsvetsinskaya et al. (2001) made the first attempt to integrate a corn simulation model into a physical and soil hydrological model, BATs (Dickinson et al., 1993). The coupled model was able to capture the seasonal change in LAI for corn and the results demonstrate its importance for the calculation

of the surface fluxes of heat, moisture and momentum. The IBIS was extended to include crops (Donner and Kucharik, 2003) and validated and applied to simulate crop yields, water and energy balance and impacts of agricultural management (Kucharik, 2003; Sachs and Kucharik, 2011). Gervois et al. (2004) implemented a crop simulation model (STICS) (Brission et al., 2002) in ORCHIDEE land surface model (Krinner et al., 2005) to specifically simulate winter wheat and maize in two sites in Western Europe and two sites in the US. Bondeau et al. (2007) have implemented a dynamic representation of carbon allocation, phenology and management practices for a number of crops into LPJ-DGVMs (Sitch et al., 2003). Lokupitiya et al. (2009) developed crop-specific phenology and coupled them to SiB (Sellers et al., 1996a,b). Van den Hoof et al. (2011) implemented dynamic crop growth structure and phenology into JULES-SUCROS (Cox et al., 1999) to study the impact of interactive effect of wheat structure and phenology on land–atmosphere interactions. Most recently, the carbon allocation and phenology algorithms for corn, soybean and temperate cereals of Agro-IBIS model (Kucharik and Byre, 2003) have been introduced into the Community Land Model's (CLM's) (Lawrence et al., 2012) to examine the effects of managed crops on climate (Levis et al., 2012).

This paper builds upon and extends the approaches of the studies discussed above. While we use a similar carbon assimilation, energy and hydrological modeling approach, we implement new algorithms to simulate the following processes: (i) crop growth and biomass allocation in five phenology stages, distributing assimilated carbon among above and below ground parts depending upon both the accumulated heat and the resource availability, such as light, water, and nutrient (e.g., nitrogen); (ii) development of vegetation structure (LAI, canopy height and root depth) calculated based on accumulated carbon mass in leaf, stem and root pools; (iii) vertical and horizontal root growth in soil layers in response to available soil moisture; and (iv) different abscission rates for fresh and old dead leaves. Following these implementations, the model parameters were calibrated and model performance was evaluated using observational

data (LAI, biomass, and carbon, water and energy fluxes) from two AmeriFlux sites (Mead, NE and Bondville, IL) under corn-soybean rotation system.

The implementation of these new processes into ISAM improved the model predictions relative to observations, such as the estimates of energy and water fluxes from land surfaces and their feedbacks with environmental variables. For example, dynamic carbon allocation and vegetation structure allow simulation of seasonal vegetation structural changes with environmental condition. With dynamic root distribution schemes, the model is able to simulate the root response to soil water availability in each soil layer and accounts for redistribution of soil water by root systems and strengthens the model ability to simulate crop growth under dry conditions. Also, the different abscission rates for fresh and old standing dead leaves distinguish two steps of leaf senescence; color change (green to brown) and leaves falling, and better represent water and energy interception by both stem and brown leaves of the canopy during leaf senescence.

2 Model description

ISAM is a coupled biogeochemical and biogeophysical model with $0.5° \times 0.5°$ spatial and multi-temporal resolution from half-hour to year (Jain and Yang, 2009; Yang et al., 2009; El-Masri et al., 2013). Each grid cell is occupied by a combination of fractional vegetation, bare soil, and glacier (Meiyappan and Jain, 2012). Here we add two crop functional types (corn and soybean) into the model. There are sunlit/shaded canopy, 10 hydrological and thermal active soil layers, five hydrological and thermal inactive bedrock layers, seven vegetation pools and eight litter and soil organic matter (SOM) pools in the ISAM (Yang et al., 2009; El-Masri et al., 2013). Carbon assimilation, heat and water fluxes are calculated through coupled canopy photosynthesis, energy and hydrological process. Carbon assimilation is allocated into seven vegetation pools and eight litter and soil organic matter (SOM) pools and further coupled with complete N

cycle process, including N deposition, N fixation, N mineralization, N immobilization, nitrification, denitrification and leaching (Yang et al., 2009).

The model variables, parameters and equations are given in Tables A1 and A2.

2.1 Coupled canopy photosynthesis, energy and hydrological balance processes

Carbon assimilation rates, energy and water fluxes are calculated by coupling a leaf temperature, photosynthesis and stomatal conductance model (Dai et al., 2004; Chen et al., 2010) with an energy and hydrological balance model (Dai et al., 2004; Oleson et al., 2004, 2008).

The carbon assimilation model is composed of a variant of the Ball-Berry stomatal conductance model (Ball et al., 1987; Collatz et al., 1991), the C3 photosynthesis model (Farquhar et al., 1980; Collatz et al., 1991) and the C4 photosynthesis model (Collatz et al., 1992). The stomatal conductance is calculated as the function of net carbon assimilation rate, relative humidity and CO_2 concentration at the leaf surface. C3 carbon assimilation rate is co-limited by light availability, Rubisco efficiency and ability of carbon compound export. C4 carbon assimilation rate is co-limited by light availability, Rubisco efficiency and PEP-Carboxylase availability.

The CO_2 compensation point for C3 biome in original ISAM was calculated as a function of O_2 partial pressure and temperature-dependent Rubsico specificity for CO_2 relative to O_2 (Dai et al., 2003). However, this method underestimated the compensation point during the beginning and end of growing season, resulting in the higher GPP than observed during these two stages of the growing season. Smith et al. (1976) suggested that the compensation point for the young leaves was higher and decreased when the leaves grew, stayed constant after maturity, and increased again during senescence. Following Smith et al. (1976), we calculated the rate of change of compensation point as function of leaf age.

Temperature regulates carbon assimilation processes by multiplying temperature functions (Dai et al., 2003) with the maximum carboxylation rate at the reference tem-

perature of 25 °C (V_{cmax25}). The effect of soil water availability on carbon assimilation is dependent on V_{cmax25} and dark respiration and minimum stomatal conductance (Oleson et al., 2008). Moreover, seasonal variation in V_{cmax25} is calculated based on day length factor (Bonan et al., 2011).

5   Leaf level photosynthesis and stomatal conductance are scaled to canopy level separately for sunlit and shaded leaves by using sun/shade canopy LAI fractions and scaling parameters to represent extinction of nitrogen and light through the vertical canopy (Dai et al., 2004). A detailed documentation of carbon cycle equations in the current ISAM is documented in El-Masri et al. (2013).

10   Energy conservation of the soil-vegetation system in the ISAM is calculated as the balance of absorption of net shortwave and long-wave radiation (Rn) by sunlit/shade canopy and ground, and emissions of sensible (*H*) and latent heat (LH) fluxes from leaves and ground and soil heat fluxes (*G*). The net solar radiation is calculated by two-stream approximation (Sellers et al., 1996a), which dynamically calculates the in-

15 terception, reflectance, transmission and absorption of direct and diffuse radiation by sunlit/shaded canopy and soil (Dai et al., 2004). We further modified the treatment of diffuse radiation in the "two-stream" scheme based on Bonan et al. (2011) to reduce biases in shaded leaf photosynthesis. Vegetation optical characteristics (leaf/stem reflectivity and transmissivity, Table A1), canopy structure (expressed as leaf angle dis-

20 tribution, Table A1) and density (expressed as leaf area index (LAI) and stem are index (SAI)) dynamically control partitioning of canopy-intercepted radiation and ground-intercepted radiation, as well as partitioning of vegetation adsorbed net radiation between sunlit and shaded canopy. Sunlit canopy intercepts direct and diffuse radiation, whereas shaded canopy intercepts only diffuse radiation.

25   Latent heat transfer to atmosphere is resolved using canopy transpiration, canopy evaporation from the intercepted precipitation water, condensation of evaporated water, dew formation, and ground evaporation; sensible heat is partitioned into ground and canopy components (Dai et al., 2003). High biases in soil evaporation are reduced by imposing an additional soil resistance (Sellers et al., 1992) and a litter resistance

Full Screen / Esc

(Sakaguchi et al., 2009) to the humidity transfer from ground to atmosphere. Convergence of aerodynamic properties from thick/thin canopies to that of ground is ensured based on Zeng and Wang (2007). Surface albedo is resolved into ground albedo (function of soil color and wetness), exposed vegetation albedo (function of leaf orientation, leaf/stem reflectivity and transmissivity, and ground albedo), and snow albedo (Zeng et al., 2002).

Hydrological cycle is coupled with energy cycle through latent heat of evaporation from wet canopy and ground, transpiration from dry canopy, and water content-adjusted soil heat conductivity. Canopy interception and throughfall of precipitation, infiltration, redistribution of soil water within the soil column, surface runoff and subsurface percolation are calculated using the formulations of Oleson et al. (2004, 2008). Canopy interception of precipitation and dew formation, as a function of canopy density, determines dry/wet fraction of canopy and thus partitioning of evaporation and transpiration from leaves. These processes are coupled with dynamic root distribution algorithm (Arora and Boer, 2003) and determine the soil water availability for root uptake and transpiration. The soil heat is modeled based on Fick's equation (Dai et al., 2003), whereas soil water flux is implemented based on Richard's equations (Oleson et al., 2004). The thermal and hydrological properties for each soil layer are estimated based on soil liquid and ice water contents, soil temperature, soil texture and soil organic carbon (SOC) and gravel content (Lawrence et al., 2008). The soil texture data is from IGBP-DIS $0.5° \times 0.5°$ dataset (Global Soil Data Task Group, 2000), whereas SOC and gravel content data are taken from Harmonized World Soil Database (HWSD) (FAO/IIASA/ISRIC/ISSCAS/JRC, 2012).

2.2 Dynamic crop growth processes

2.2.1 Phenology development

The crop phenology begins with planting of seeds and ends with grain harvest. In between, the phenology is divided into five growth stages: emergence period, initial vege-

tative period, normal vegetative period, initial reproductive period and post-reproductive period.

The planting date is determined when the following three conditions are satisfied simultaneously (Eq. A1): (1) mean daily air temperature of past seven consecutive-days is greater than the base temperature (T_{base}); (2) mean daily soil temperature of past seven consecutive days is greater than the crop-specific critical soil temperature for emergence ($T soil_{critical}$); (3) accumulated growing degree days above 0 °C is greater than the crop-specific minimum value ($GDD0_{min}$) (Eq. A1). At the time of planting, the seeding rate is given as an input parameter based on field crop management. After planting, the transition of the different growth stages of phenology is determined by the heat unit index (HUI) and the accumulated days for each growth stage (Eqs. A2–A7). The HUI is 0 at the planting time and 1 at the time the crop matures. The required heat value and the total numbers of days for each growth stage are attained from published studies (Darby and Lauer, 2000; McWilliams et al., 2004; USDA-NASS, 2009; USDA-OCE, 2010). These values are further calibrated based on multiyear LAI from Mead, NE AmriFlux site (Verma et al., 2005). Moreover, LAI is also used to determine the transition from vegetative to reproductive growth (Eqs. A3–A7). The model also accounts for extreme cold and warm temperatures on crop yields. The effect of colder temperature on yield is accounted for by assuming 100 % loss of yield when the mean daily temperature for five consecutive days falls below 273.2 K (Darby and Lauer, 2000) (Eq. A8).

When severe drought stress occurs, silk emergence is delayed during the reproductive period. This effect severely decreases corn yields. This effect is activated in the model when the following two conditions are met simultaneously (Eq. A9): (1) mean daily temperature of three consecutive days reaches above 303.2 K (Shaw, 1988; Rattalino Edreira and Otegui, 2012); (2) mean water stress index of three consecutive days is lower than 0.5. Finally, the crops are harvested when they get matured, i.e., HUI = 1.0.

2.2.2 Carbon allocation

An assimilated carbon in leaves is allocated to stems, roots and grain. The leaf component is divided into photosynthetically active (green leaves) and dead (senescent) leaves. The initial carbon is determined based on the amount of carbon stored in the seeds (Eq. A10). During the emergence time carbon stored in seed is allocated to leaf and root based on thermal conditions (Eq. A11). The carbon assimilation through photosynthesis allocates carbon to each vegetation pool (leaf, stem, root and grain) (Eqs. A18–A21). Part of the assimilated carbon is lost through respiration (Eq. A12). Maintenance respiration for each vegetation pool is calculated as the function of carbon amount, the C : N ratio and temperature-depended respiration coefficients (Eq. A13) (Sitch et al., 2003). Temperature-depended respiration coefficients are calculated based on a specified respiration rate at 20 °C and a Q_{10} temperature function (Arora et al., 2003) (Eq. A14). The Q_{10} values for leaf, stem and root respiration are calculated as a function of leaf, stem and soil maintenance temperature, respectively (Arora et al., 2003) (Eq. A15). The growth respiration is assumed to be 25 % of the remainder after removing maintenance respiration from GPP (Eq. A16). The partitioning of the growth respiration into each vegetation pool follows the fraction of carbon amount in each vegetation pool (Eq. A17).

The net assimilated carbon (GPP minus maintenance and growth respirations) allocated to leaf, stem, root and grain pools is a dynamic process based on temperature, water availability, light and N to alter the carbon allocation fractions dynamically at each model time step (Eq. A22). The objective of this allocation scheme is that the allocation of carbon into leaves, stems, and roots are adjusted to minimize adverse effects of limited availability of light, water, and mineral nutrients. Accordingly, more carbon is allocated to roots when soil moisture and mineral N are limiting, or to stem and leaf when the increase in leaves results in a decrease in light penetrating the canopy (Arora and Boer, 2005; Salter et al., 2003). This dynamic allocation approach is similar to that of Friedlingstein et al. (1999) and Arora and Boer (2005), except that carbon allocation

Title Page

Abstract | Introduction

Conclusions | References

Tables | Figures

◄ | ►►

◄ | ►

Back | Close

Full Screen / Esc

Printer-friendly Version

Interactive Discussion

factors for the different stages of phenology vary with HUI (Eqs. A18–A26) based on Penning de Vries et al. (1989).

During the vegetative period, allocated carbon in the green leaf and stem increases with HUI in order for the canopy to build and capture increasing amounts of radiation (Eqs. A19 and A25). There is no new carbon allocated to the green leaf pool in the initial and post reproductive period. Instead, leaf pool loses carbon through maintenance respiration (Eq. A26), and the carbon is allocated to grain with increasing HUI to increase grain filling during initial reproductive period (Eq. A26). However, no C is allocated to corn grain if the silk emergence is delayed under the drought conditions.

The transition from vegetative period to reproductive period initiates the process of leaf senescence. During this period, green leaf carbon is reduced, leading to reduced photosynthetic carbon fixation. The conversion of green leaf carbon to dead leaf carbon occurs at death rates that vary due to drought or cold condition following the formulations of Arora and Boer (2005) (Eqs. A27–A30).

During the post reproductive period, assimilated carbon is only allocated to grain and root pools (Eq. A21). If no green leaves exist before crop maturity, carbon stored in roots and stems is partly reallocated to the grain pool to enhance the grain filling. In order to account for the effect of water stress on grain filling, the reallocation fraction factor is downscaled (Eq. A26).

Finally, a dynamic allocation factor for each vegetation pool is modified to satisfy two conditions (Arora and Boer, 2005). The first is that there must be enough root and stem biomass to support leaf biomass (Eq. A31). A second condition is that a minimum root/shoot ratio must be available to maintain the structure of each crop type (Eq. A32). If the first condition is not satisfied, the carbon is allocated to root and stem. If the second condition fails to attain, carbon is allocated to root. A fraction of the carbon allocated to the vegetation pools can be lost as litter. Following Arora and Boer, (2005), conversion of the root and stem carbon to litter occurs at a fixed turnover rate (Eqs. A33–A34). Conversion of dead leaves to litter occurs as a function of fresh dead leaves and accumulated dead leaves produced in previous time steps (Eq. A35).

Implementation of dynamic crop growth processes into a land surface model

Y. Song et al.

2.2.3 Calculation of LAI, canopy height and root depth

LAI is calculated as a function of leaf carbon and *SLA* (Eq. A36). ISAM model partitions the total LAI between green LAI and dead LAI (Eqs. A37–A38). Canopy height is calculated as a function of aboveground biomass (Arora and Boer, 2005) (Eq. A39). Root depth and root fraction in each soil layer varies temporally and spatially with root biomass (Arora and Boer, 2003) (Eqs. A40–A43).

3 Model calibration and evaluation methods using Ameri-Flux and other data sets

Field data for corn and soybean from two AmeriFlux eddy covariance flux tower sites under corn and soybean rotation in the US Midwest were used to evaluate the performance of the ISAM model. The hourly-measured carbon, heat and water exchanges between atmosphere and canopy, and biweekly-measured LAI, leaf carbon, biomass and annual yield (ftp://cdiac.ornl.gov/pub/ameriflux/data/Level2/Sites_ByName/Mead_Rainfed/) at Mead rainfed site, Nebraska (41.18° N, 96.44° W) (Suyker et al., 2004), are used to calibrate the following ISAM model parameters: GDD_{max}, $GDD0_{min}$, SLA, initial carbon allocation fraction for each phenology stage (Eqs. A20–A25), minimum HUI during each phenology stage (Eqs. A3–A7), and parameters in litter production functions (Eqs. A33–A35) and canopy height function (Eq. A39). The measurement data (ftp://cdiac.ornl.gov/pub/ameriflux/data/Level2/Sites_ByName/Bondville/) for another US Midwest site at Bondivlle, Illinois (40.00° N, 88.29° W) (Hollinger et al., 2005) are used to evaluate the model performance for carbon (GPP) and energy fluxes (net radiation (Rn) at the top of canopy, latent heat (LH) and sensible heat (*H*) fluxes) between atmosphere and canopy at both diurnal and seasonal scale, and seasonal LAI.

The two sites have distinct climate and soil characteristics. The Mead, Nebraska rainfed site sits on deep silt clay loam (Suyker et al., 2004). Mean precipitation and temperature during the four growing seasons (2001–2004) used in this study were

370 mm and 21.1°, respectively. The Bondville, Illinois site is relatively moist with mean precipitation and air temperature of 398 mm and 20.9°, respectively for the 2001–2004 growing season. The soil type for the Bondville site is silt loam (Hollinger et al., 2005), which has larger soil water holding capacity than that of Mead site. The Mead and Bondville sites have been planted with corn and soybean in rotation since 2001 and 1996 year, respectively. Weeds are controlled with herbicides, but no tillage or irrigation is used at either site (Meyers and Hollinger, 2004; Suyker and Verma, 2009).

3.1 Model experiments

We spin-up the model for each site with corn-soybean rotation under repeating site climate data from 2001 to 2004 years until the soil temperature and moisture reach the steady state. Then, we run the model with site-specific planting and harvest times from 2001 to 2004 year to calibrate and evaluate the model performance. Due to lack of measured energy balance closure at many sites (Wilson et al., 2002), we perform the energy balance closure correction according to Twine et al. (2000), which preserves the Bowen ratio:

$$f = \frac{\sum (Rn - G - S)}{\sum (H + LH)} \tag{1}$$

Here f is the correction factor. The corrected LH or H is calculated by multiplying the measured LH and H fluxes with f. All the energy flux terms, except for storage energy term (S), are measured at the two sites. We assume S for the Bondville site to be 14 % and 8 % of Rn for corn and soybean, respectively (Meyers and Hollinger, 2004). For the Mead site, Suyker and Verma (2010) have estimated the corrected energy fluxes for the period 2001–2006, which we apply here.

3.2 Statistics analysis

The continued hourly/half-hourly observed fluxes have non-random errors and biases (Williams et al., 2009). Therefore, the regression analysis is not an optimal way to

analyze the model performance. Instead, we use the refined Willmott's index (Willmott et al., 2012) method to quantify the degree to which observed hourly GPP, energy and water fluxes are captured by the model. The refined Willmott's index is calculated as:

$$dr = \begin{cases} 1 - \sum_{i=1}^{N} |P_i - O_i| / 2\sum_{i=1}^{N} |O_i - \bar{O}| & \text{if } \sum_{i=1}^{N} |P_i - O_i| \leq 2\sum_{i=1}^{N} |O_i - \bar{O}| \\ 2\sum_{i=1}^{N} |O_i - \bar{O}| / \sum_{i=1}^{N} |P_i - O_i| - 1 & \text{if } \sum_{i=1}^{N} |P_i - O_i| > 2\sum_{i=1}^{N} |O_i - \bar{O}| \end{cases} \qquad (2)$$

Here P_i and O_i are the individual modeled and observed data respectively. $\bar{O}$ is the mean of the observed values. N is the number of the paired observation and modeled data. The $\sum_{i=1}^{N} |P_i - O_i|$ part (Eq. 2) represents the sum of modeled error magnitude, and the $2\sum_{i=1}^{N} |O_i - \bar{O}|$ part (Eq. 2) represents the sum of the perfect modeled-deviation and observed-deviation (Willmott et al., 2012). The range of refined Willmott's index, dr, is from −1 to 1. A dr of 1 indicates perfect agreement between model and observation, and a dr of −1 indicates either lack of agreement between the model and observation or insufficient variation in observations to adequately test the model. Here we calculated dr for hourly observed and modeled data, dr_h, to examine the degree to which the model represents the hourly variation in observed values. For the Bondville site, the half-hourly observed and modeled data are accumulated to hourly data and then used to calculate dr_h. We also calculated dr for daily mean observed and modeled data, dr_d, to examine the model performance at daily time scale. The comparison of dr_h and dr_d allowed us to evaluate model biases at these different time scales.

In addition, instantaneous soil moisture measured at the AmeriFlux sites were used to evaluate the modeled soil moisture.

Back | Close

Full Screen / Esc

Printer-friendly Version

Interactive Discussion

4 Results and discussion

4.1 Calculations of GPP, water fluxes and energy exchange between atmosphere and canopy

Table 1 shows the statistical analysis and Figs. 1 and 2 compare modeled and measured data for GPP, energy fluxes (Rn, LH and H) over the period 2001–2004. The statistical analysis and direct model-data comparison results suggest that model estimated carbon assimilation and energy and water fluxes, with the exception of sensible heat flux at both sites, are in good agreement with observations. The relatively low dr_h and dr_d values were found for H under corn and soybean rotation at both sites, suggesting that modeled results are not consistent with observations. The possible reasons for the differences are discussed below.

The model is also able to capture the basic daily variation in soil moisture under corn and soybean rotation during growing period 2001–2004 at both sites (Fig. 2e, j, o, t). The results related to the parameterization of corn and soybean root profile are further discussed in Sect. 4.2. The model estimated LAI are also consistent with the observation data (Fig. S1).

4.1.1 GPP

The dr_h for GPP under corn and soybean rotation varies from 0.82 to 0.86 at both sites (Table 1), indicating that model estimated hourly GPP variations for most cases are consistent with the observations (Fig. 1a, e, i, m). The model results for soybean GPP were improved by regulating CO_2 compensation point with leaf age. For example, the implementation of leaf age effect on CO_2 compensation point effectively reduced simulated soybean GPP not only at the calibrated Mead site, but also at the Bondville site and these downscaled values are in much better agreement with the measured values during the leaf expansion period (Fig. S2). The dr_d values for GPP under corn and soybean rotation varies between 0.71 and 0.92, suggesting that the model estimated

daily GPP for most of the cases are consistent with the observations (Fig. 2 a, f, k, p). The dr_d values are lower than the dr_h values for corn at Bondville, indicating that the model estimates are less consistent with the measured values during certain time period of the growing season. Figure 2k suggests that the model fails to capture a sharp reduction in GPP during the initial reproductive period of 2003 (between Julian day 202 and 215). The reason for the sharp reduction in observed GPP is unknown, but the Illinois water and climate summary on July 2003 reports widespread crop lodging due to gusty wind during this period in central Illinois (Winstanley, 2003). The weather report at the nearest weather station (40.03° N, 88.28° W) (http://www.tutiempo.net/en/Climate/ Champaign_Urbana_University_Of_Illinois-Willard_Airport/07-2003/725315.htm) also suggests that area received a thunderstorm with wind gusts over 30 mph on Julian day 202 of 2003 and wind gusts (> 30 mph) between Julian day 203 and 208 of 2003 and the high wind gust might have induced the crop lodging and hence reduced the GPP. The model is unable to capture this information, because the model is not currently accounting for the effect of extreme gust on crop.

4.1.2 *H* and LH fluxes

The dr_h for corn and soybean *H* have the same value of 0.68 at Mead site and 0.60 and 0.69 at Bondville site, suggesting that there are model biases in hourly *H* at both sites. However, the dr_h for corn-soybean LH at Mead and Bondville sites are much higher than for *H* and vary between 0.84–0.86 and 0.83–0.84, respectively. These higher values of dr_h suggest that the model is able to capture most of variation in observed hourly LH at both sites (Fig. 1d, h, l, p). The apparent model errors in hourly *H* are usually occur due to errors in modeled hourly LH (Fig. 1d, h, l, p) and Rn (Fig. 1b, f, j, n). The error in modeled *H* is more apparent at the diurnal level at both sites and in modeled diurnal LH, particularly at Mead site. The model overestimates *H* during the morning hours (UTC 06:00–10:00 a.m.), but slightly underestimates *H* during the afternoon hours (after UTC 02:00 p.m.) (Fig. 1c, g, k and o) at both sites. Similar errors in modeled LH are observed at Mead site (Fig. 1d and h). These model discrepancies are related to

smaller model biases in Rn (Fig. 1b, f, j and n), which introduce quite a large error in modeled H and LH. The overestimated Rn speeds up the penetration of the stable stratified canopy atmosphere during the morning hours and warms the canopy quickly, leading to a sudden increase in H and LH fluxes after sunrise. The biases in modeled H are also observed during the night hours at the Bondville site when the model usually simulates negative H, instead of mean zero value of H in the measurement. Note that the negative modeled H indicates the existence of stable stratified atmospheric layers during the night time. It is important to note that observed fluxes through the eddy covariance technique are usually unreliable during night hours (Goulden et al., 1996), that also add to discrepancy between modeled and observed values.

The estimated dr_d values for H and LH fluxes are higher than dr_h values for corn at Mead site and soybean at Bondville site, indicates that the model is able to capture the daily pattern in energy fluxes much better than that of hourly fluxes (Fig. 2c–d and r–s). However, the model biases in H and LH are apparently observed during specific time period for soybean at Mead and corn at Bondville, as indicated by the lower dr_d values than the dr_h values at two sites (Table 1). The overestimated H and underestimated LH are observed during the normal vegetative period and the initial reproductive period in 2002 at Mead site (Fig. 2h). This model discrepancy results from underestimated soil water content during dry period (Fig. 2j), when underestimated soil water reduces the water availability for evapotranspiration, leading to an underestimation of LH flux through evapotranspiration, but at the same time overestimation of H. The similar partitioning discrepancy between H and LH is also observed during the normal vegetative period of 2001 corn growing season and at the end of 2003 corn growing season at Bondville (Fig. 2m–n). The results point to the need to explore this issue further in order to improve the representation of the surface energy exchanges. Moreover, the forced energy balanced closure of measured data, which distributes unbalanced energy into H and LH based on Bowen ration, also could introduce uncertainty in measured H and LH and thus contribute to discrepancy between modeled and measured fluxes. Besides sampling errors associated with measured values for Rn, H and LH, the turbulent ex-

change of the smaller eddies with larger eddies on larger scales of the heterogeneous landscape can also induce the error in estimated energy balance closure (Wilson et al., 2002; Foken, 2008). In addition, as pointed out by Wilson et al. (2002), the Bowen ratio method (Eq. 1) might have overlooked the biases in the half-hourly/hourly data, such as the tendency to overestimation of positive fluxes during daytime and underestimation negative fluxes during nighttime.

4.2 The effects of dynamic carbon and root distribution on modeled results

To address the importance of dynamic carbon allocation and root distribution parameterizations on modeled carbon and energy fluxes, especially under water stress conditions, we ran the model with dynamic root distribution (ISAM-DynamicR) and static root distribution (ISAM-StaticR) schemes, respectively. The ISAM-StaticR refers to predetermined root depth and root fraction for each soil layer in space and time that develops independent of soil and water conditions (Schenk and Jackson, 2002). ISAM-DynamicR accounts for variability of root distribution (that is root depth and root fraction for each layer) as a function of soil water in space and time. The static root distribution function parameters for corn and soybean are assumed to be the same as those for all annual plants (Schenk and Jackson, 2002). This function was used to define the root distribution for the generic crop in the original version of the ISAM (El-Maseri et al., 2013). This method has also been used to define the root distribution for the crops in most of the land surface models.

As discussed in Sect. 3, the root distribution for ISAM-dynamicR is calculated based on Eqs. (A40)–(A42). There is not much information available in literature about the root distributions for corn and soybean to calibrate and validate the modeled dynamic root distributions. While the data is not available for the growing season studied here, corn root profiles on three specific dates in 1980 were measured at Mead site (Newell and Wilhelm, 1987), which we have used to calibrate two parameters (root growth direction parameter (α) and root distribution parameter (bb)) for corn in dynamic root distribution functions (Eqs. A41–42). For soybean, we calibrate α and bb by comparing

measured and modeled soil water content. In order to evaluate the performance of model parameterization for other times and space in Midwest region, we compared modeled total growing season GPP and LH for ISAM-DynamicR and ISAM-StaticR cases with measurement over the period 2001–2004 at Mead and Bondville sites.

In order to illustrate the importance of dynamic root characteristics, here we compare the model estimated water uptake for ISAM-DynamicR and ISAM-StaticR cases for year 1980 at Mead site. Due to lack of site-specific climate forcing data in 1980, we use 1980 NLDAS-2 climate forcing data (Mitchell et al., 2004) to drive the model. All other information, such as management seedling rate, planting time etc., are taken from Newell and Wilhelm (1987). Figure 3a–c shows that calibrated model for ISAM-DynamicR case captures well the measured trends of root growth with soil depth during the growing season for corn at the Mead site; whereas ISAM-StaticR case overestimates root density in shallow soil layers but underestimates in deep soil layers during the growing season. These differences in root characteristics for two parameterization cases in turn influence the estimates of simulated soil water stress and root water uptake and hence transpiration (Fig. 3d–f). This is because transpiration is more sensitive to the moisture content of the densely rooted shallow soil layers than that in the remainder of the root zone (Feddes et al., 2001). On Julian day 174 when soil moisture is optimal during initial vegetative stage, the calculated total amount of root water uptake for both cases are approximately the same ($2.33\,\text{mm day}^{-1}$), but there are substantial differences in the magnitude of the water uptake at different soil depths, specifically in the shallow soil layers. For the ISAM-StaticR case maximum amount of water is extracted from shallow soil layers above 0.03 m, whereas for ISAM-DynamicR case roots take water from the more moisture deeper layers above 0.12 m (Fig. 3d). However, ISAM-StaticR parameterization overestimates the root density and water uptake in shallow layers (Fig. 3b, c), reducing the soil water available in the shallow soil as the growing season progresses. This results in an earlier and more intense start of soil moisture stress and lower actual transpiration in ISAM-StaticR case than that in ISAM-DynmaicR case (Fig. 3e, f). In order to illustrate the importance these results

Full Screen / Esc

Printer-friendly Version

Interactive Discussion

with time, here we show the ISAM results for the year 2001 corn-growing season at Mead as an example. As the Fig. 4 shows, the transpiration is higher for the ISAM-DynmaicR than in ISAM-StaticR case during the growing season and the transpiration differences between the two cases gradually increases, especially during the summer,
5   when low summer precipitation cannot effectively compensate soil water depletion in shallow layers (not shown here). The increased water uptake from deeper and moist root zone in ISAM-DynamicR case mitigates the intensity of water stress during the growing season by about 60 % and improves the simulations of soil water uptake in when soil water in the upper soil layers is exhausted during the growing season.
10   In order to evaluate the validity of the dynamic root parameterization scheme, we compare model results for total transpiration, latent heat flux and GPP during the 2001–2004 growing seasons under corn and soybean rotation at Mead and Bondville sites. The ISAM model results suggest that ISAM-DynamicR parameterization estimated plant water transpirations during 2001–2003 growing season are about 28–
15   34 % higher than ISAM-StaticR (Fig. 5a). However, there is no apparent difference in plant water transpiration between ISAM-StaticR and ISAM-DynamicR case over 2004 growing season at both sites (Fig. 5a). The increased transpiration in ISAM-DynamicR case, relative to ISAM-StaticR case, mitigates water stress effect on catalytic capacity of Rubisco (V_{cmax25}) and stomatal conductance. This results in an 13–61 % increase
20   in GPP and 12–27 % increase in LH at Mead site, and 26–41 % increase in GPP and 13–21 % increase in LH at Bondville site for ISAM-DynamicR case relative to the ISAM-StaticR case (Fig. 5b, c). The increased values for GPP and LH for ISAM-DynamicR case are in much better agreement with observations (Fig. 5b, c) than for ISAM-StaticR case. Moreover, the dr_d and dr_h values for GPP and LH (Table 2) are much closer to
25   1 in ISAM-DynamicR case than that in ISAM-StaticR case for most of the cases. One particular exceptional case is corn GPP at Bondville site. As discussed in Sect. 4.1, model is not able to capture a sharp reduction in corn GPP during this year, and thus overestimates corn GPP at Bondville site. While ISAM-DynamicR case mitigates downscaled effects of water stress on GPP and thus further overestimates GPP (Fig. 5b, c).

Compared to ISAM-StaticR case, the increase in dr_d values for GPP and LH for ISAM-DynamicR case are much greater than the increase in the values of dr_h at both sites (Table 2), suggesting that ISAM-DynamicR version of the model much better captures the daily pattern of carbon, energy and water fluxes than the ISAM-StaticR version.

5   Specifically, the apparent increase in the values of dr_d for GPP and LH at Mead site (Table 2), where crops endures water stress conditions during 2001–2004 growing season, indicating the importance of dynamic carbon allocation and root distribution mechanism in the calculations of carbon, energy and water fluxes under water stress conditions.

10   5   Conclusions

We have implemented the dynamic crop growth processes into a land surface model, ISAM, which includes specific phenology development for corn and soybean, dynamic carbon allocation, vegetation structure and root distribution, as well as different removal rates for fresh and old standing brown leaves and the effects of leaf age on CO_2 com-
15   pensation point for C3 crops.

The C3 and C4 crop growth processes in the model are calibrated with half-hourly/hourly data for LAI, biomass, carbon, water and energy fluxes measured for corn-soybean rotation system at the Mead, Nebraska AmeriFlux site and the model was evaluated for the same variables using the data from another AmeriFlux site at
20   Bondville, Illinois. The calibrated and evaluated ISAM model is able to capture the diurnal and growing season patterns of carbon assimilation, water and energy fluxes for corn (C4 crop) and soybean (C3 crop) at these two sites. Specifically, the calculated GPP, Rn and LH fluxes compared well with observations, but the model is unable to capture the variation in H flux for corn and soybean at both sites as discussed in
25   Sect. 4.1.

The model with dynamic carbon allocation parameterization and dynamic root distribution captures well the measured seasonal pattern of vegetation structures, in partic-

ular changes in LAI and the vertical distribution of root in soil. The improved crop water transpiration and soil water stress significantly improve modeled GPP and LH, especially during dry period. The percent differences between the estimated fluxes based on dynamic and static cases for LH were 12–27 % and for GPP 13–62 % at Mead and Bondville sites. These results indicate the importance of considering dynamic allocation and root distribution process into the land surface model to accurately simulate the carbon, water and energy fluxes, especially during dry period. The consideration of different removal rates for fresh and old standing dead leaves improves the model representation of green and brown leaves on the stem during leaf senescence, and thus better represents water and energy interception by both stem and brown leaves of the canopy, leading to improved GPP and LH simulation. The incorporation of the effect of leaf age on CO_2 compensation point effectively reduces the modeled GPP and LH fluxes for soybean during the initial vegetative and leaf senescence period.

Though measured bias for most of energy fluxes, except for H, is within the range of measured uncertainty, accurate comparison between measured and simulated energy fluxes and further understanding of model biases in partitioning H and LH is needed to evaluate the model bias of sensible fluxes.

In the future studies, the model will be applied to assess the interaction between crop growth and climate change. Since we have developed a flexible process-based framework for simulating the growth of different crop species, such as wheat, or energy crops, such as Miscanthus and switchgrass, will be implemented in ISAM.

Supplementary material related to this article is available online at: http://www.biogeosciences-discuss.net/10/9897/2013/ bgd-10-9897-2013-supplement.pdf.

Title Page

Abstract | Introduction

Conclusions | References

Tables | Figures

◄ | ►

◄ | ►

Back | Close

Full Screen / Esc

Printer-friendly Version

Interactive Discussion

References

Arora, V. K.: Simulating energy and carbon fluxes over winter wheat using coupled land surface and terrestrial ecosystem models, Agr. Forest Meteorol., 118, 21–47, 2003.

Arora, V. K. and Boer, G. J.: A representation of variable root distribution in dynamic vegetation models, Earth Interact., 7, 1–19, 2003.

Arora, V. K. and Boer, G. J.: A parameterization of leaf phenology for the terrestrial ecosystem component of climate models, Glob. Change Biol., 11, 39–59, 2005.

Ball, J. T., Woodrow, I. E., and Berry, J. A.: A model predicting stomatal conductance and its contribution to the control of photosynthesis under different environmental conditions, in: Progress in Photosynthesis Research, edited by: Biggins, J., Martinus Nijhoff, Dordrecht, Netherlands, 221–224, 1987.

Bernacchi, C. J., Morgan, P. B., Ort, D. R., and Long, S. P.: The growth of soybean under free air [CO_2] enrichment (FACE) stimulates photosynthesis while decreasing in vivo Rubisco capacity, Planta, 220, 434–446, 2005.

Bonan, G.: Forests and climate change: forcings, feedbacks, and the climate benefits of forests, Science, 320, 1444–1449, 2008.

Bonan, G. B., Lawrence, P. J., Oleson, K. W., Levis, S., Jung, M., Reichstein, M., Lawrence, D. M., and Swenson, S. C.: Improving canopy processes in the Community Land Model version 4 (CLM4) using global flux fields empirically inferred from FLUXNET data, J. Geophys. Res., 116, G02014, doi:10.1029/2010JG001593, 2011.

Bondeau, A., Smith, P. C., Zaehle, S., Schaphoff, S., Lucht, W., Cramer, W., Gerten, D., Lotze-Campen, H., Müller, C., Reichstein, M., and Smith, B.: Modelling the role of agriculture for the 20th century global terrestrial carbon balance, Glob. Change Biol., 13, 679–706, 2007.

Brisson, N., Mary, B., Ripoche, D., Jeuffroy, M. H., Ruget, F., Nicoullaud, B., Gate, P., Devienne-Barret, F., Antonioletti, R., Durr, C., Richard, G., Beaudoin, N., Recous, S., Tayot, X., Plenet, D., Cellier, P., Machet, J., Meynard, J. M., and Delecolle, R.: STICS: A generic model for the simulation of crops and their water and nitrogen balances. I. Theory and parameterization applied to wheat and maize, Agronomie, 18, 311–346, 1998.

Brovkin, V., Claussen, M., Driesschaert, E., Fichefet, T., Kicklighter, D., Loutre, M. F., Matthews, H. D., Ramankutty, N., Schaeffer, M., and Sokolov, A.: Biogeophysical effects of historical land cover changes simulated by six Earth system models of intermediate complexity, Clim. Dynam., 26, 587–600, 2006.

Title Page

Abstract | Introduction

Conclusions | References

Tables | Figures

◄ | ►

Back | Close

Full Screen / Esc

Printer-friendly Version

Interactive Discussion

Climate Champaign/Urbana, University of Illinois-Willard Airport: http://www.tutiempo.net/en/Climate/Champaign_Urbana_University_Of_Illinois-Willard_Airport/07-2003/725315.htm, 2003.

Collatz, G. J., Ball, J. T., Griver, C., and Berry, J. A.: Physiological and environmental regulation of stomatal conductance, photosynthesis, and transpiration: a model that includes a laminar boundary layer, Agr. Forest Meteorol., 54, 107–136, 1991.

Cox, P. M., Betts, R. A., Bunton, C. B., Essery, R. L. H., Rowntree, P. R., and Smith, J.: The impact of new lands surface physics on the GCM simulation of climate and climate sensitivity, Clim. Dynam., 151, 137–153, 2011.

Dai, Y., Zeng, X., Dickinson, R. E., Baker, I., Bonan, G. B., Bosilovich, M. G., Denning, A. S., Dirmeyer, P. A., Houser, P. R., Niu, G., Oleson., K. W., Schlosser, C. A., and Yang, Z.: The common land model, B. Am. Meteorol. Soc., 84, 1013–1023, 2003.

Dai, Y., Dickinson, R. E., and Wang, Y. P.: A two-big-leaf model for canopy temperature, photosynthesis, and stomatal conductance, J. Climate, 17, 2281–2299, 2004.

Darby, H. and Lauer, J.: Critical stages in the life of a corn plant, UW crop scouting manual, UWEX Publications, Madison, WI, 2010.

Dickinson, R. E., Henderson-Sellers, A. H., and Kennedy, P. J.: Biosphere-atmosphere transfer scheme (BATS) Version le as coupled to the NCAR Community Climate Model, NCAR Tech Note 387, Boulder, CO, 72 pp., 1993.

Donner, S. D. and Kucharik, C. J.: Evaluating the impacts of land management and climate variability on crop production and nitrate export across the Upper Mississippi Basin, Global Biogeochem. Cy., 17, 1085, doi:10.1029/2001GB001808, 2003.

El-Masri, B., Jain, A. K., Barman, R., Meiyappan, P., Song, Y., and Liang, M.: Carbon dynamics in the Amazonian basin: integration of eddy covariance and ecophysiological data with a land surface model, Agr. Forest Meteorol., doi:10.1016/j.agrformet.2013.03.011, 2013.

FAO: The State of food and agriculture, Food and agriculture organization of the United Nations, Rome, Italy, 1–131, 2008.

FAO/IIASA/ISRIC/ISSCAS/JRC: Harmonized World Soil Database (version 1.2). FAO, Rome, Italy and IIASA, Laxenburg, Austria, 2012.

Farquhar, G. D., von Caemmerer, S., and Berry, J. A.: A biochemical model of photosynthetic CO_2 assimilation in leaves of C_3 species, Planta, 149, 78–90, 1980.

Feddes, R. A., Kabat, P., van Bavel, P. J. T., Bronswijk, J. J. B., and Haldirstma, J.: Modelling soil water dynamics in the unsaturated zonc-State of the art, J. Hydrol., 100, 69–111, 1988.

Title Page

Abstract | Introduction

Conclusions | References

Tables | Figures

◄ | ►►

◄ | ►

Back | Close

Full Screen / Esc

Printer-friendly Version

Interactive Discussion

Foken, T.: the energy balance closure problem: an overview, Ecol. Appl., 18, 1351–1367, 2008.

Foley, J. A., Defries, R., Asner, G. P., Barford, C., Bonan, G., Carpenter, S. R., Chapin, F. S., Coe, M. T., Daily, G. C., Gibbs, H. K., Helkowski, J. H., Holloway, T., Ramankutty, N., and Snyder, P. K.: Global consequences of land use, Science, 309, 570–574, 2005.

5 Friedlingstein, P., Joel, G., Field, C. B., and Fung, I. Y.: Toward and allocation scheme for global terrestrial carbon models, Global Change Biol., 5, 755–770, 1999.

Gervois, S., de Noblet-Ducoudré, N., Viovy, N., Ciais, P., Brisson, N., Seguin, B., and Perrier, A.: Including croplands in a Global Biosphere Model: methodology and evaluation at specific sites, Earth Interact., 8, 1–25, 2004.

10 Global Soil Data Task Group: Global gridded surfaces of selected soil characteristics (IGBP-DIS), [Global Gridded Surfaces of Selected Soil Characteristics (International Geosphere-Biosphere Programme – Data and Information System)], Data set, available at: http://www.daac.ornl.gov, from Oak Ridge National Laboratory Distributed Active Archive Center, Oak Ridge, Tennessee, USA, doi:10.3334/ORNLDAAC/569, 2000.

15 Goulden, M., Munger, J., Fan, S., Daube, B., and Wofsy, S.: Measurements of carbon sequestration by long-term eddy covariance: Methods and a critical evaluation of accuracy, Global Change Biol., 2, 169–182, 1996.

Hatfield, J., Boote, K., Fay, P., Hahn, L., Izaurralde, C., Kimball, B. A., Mader, T., Morgan, J., Ort, D., Polley, W., Thomson, A., and Wolfe, D.: Agriculture, in: The effects of climate change on agriculture, land resources, water resources, and biodiversity, A report by the US Climate Change Science Program and the Subcommittee on Global Change Research, Washington, DC, USA, 362 pp., 2008.

Hofstra, G. and Hesketh, J. D.: Effects of temperature on the gas exchange of leaves in the light and dark, Planta, 85, 228–237, 1969.

25 Hollinger, S. E., Bernacchi, C. J., and Meyers, T. P.: Carbon budget of mature no-till ecosystem in North Central Region of the United States, Agr. Forest. Meteorol., 130, 59–69, 2005.

Jain, A. K., Yang, X., Kheshgi, H., McGuire, A. D., Post, W., and Kicklighter, D.: Nitrogen attenuation of terrestrial carbon cycle response environmental factors, Global Biogeochem. Cy., 23, GB4028, doi:10.1029/2009GB003519, 2009.

30 Krinner, G., Viovy, N., de Noblet-Ducoudré, N., Ogée, J., Polcher, J., Friedlingstein, P., Ciais, P., Sitch, S., and Prentice, I. C.: A dynamic global vegetation model for studies of the coupled atmosphere-biosphere system, Global Biogeochem. Cy., 19, GB1015, doi:10.1029/2003GB002199, 2005.

Kucharik, C. J.: Evaluation of a process-based agro-ecosystem model (Agro-IBIS) across the US Corn Belt: simulations of the interannual variability in maize yield, Earth Interact, 7, 1–33, 2003.

Kucharik, C. J. and Byre, K. R.: IBIS yield and nitrate leaching predictions for Wisconsin maize agroecosystems receiving varied N-fertilizer, J. Environ. Qual., 32, 247–268, 2003.

Kucharik, C. J. and Serbin, S. P.: Impacts of recent climate change on Wisconsin corn and soybean yield trends, Environ. Res. Lett., 3, 034003, doi:10.1088/1748-9326/3/3/034003, 2008.

Lawrence, D. M. and Slater, A. G.: Incorporating organic soil into a global climate model, Clim. Dynam., 30, 145–160, 2008.

Lawrence, D. M., Oleson, K. W., Flanner, M. G., Fletcher, C. G., Lawrence, P. J., Levis, S., Swenson, S. C., and Bonan, G. B.: The CCSM4 land simulation, 1850–2005: assessment of surface climate and new capabilities, J. Climate, 25, 2240–2260, 2012.

Levis, S., Bonan, G. B., Kluzek, E., Thornton, P. E., Jones, A., Sacks, W. J., and Kucharik, C. J.: Interactive crop management in the community earth system model (CESM1): seasonal influences on land-atmosphere fluxes, J. Climate, 25, 4839–4859, 2012.

Lokupitiya, E., Denning, S., Paustian, K., Baker, I., Schaefer, K., Verma, S., Meyers, T., Bernacchi, C. J., Suyker, A., and Fischer, M.: Incorporation of crop phenology in Simple Biosphere Model (SiBcrop) to improve land-atmosphere carbon exchanges from croplands, Biogeosciences, 6, 969–986, doi:10.5194/bg-6-969-2009, 2009.

Matthews, H. D., Weaver, A. J., Eby, M., and Meissner, K. J.: Natural and anthropogenic climate change: incorporating historical land cover change, vegetation dynamics and the global carbon cycle, Clim. Dynam., 22, 461–479, 2004.

McGuire, A. D., Sitch, S., Clein, J. S., Dargaville, R., Esser, G., Foley, J., Heimann, M., Joos, F., Kaplan, J., Kicklighter, D. W., Meier, R. A., Melillo, J. M., Moore III, B., Prentice, I. C., Ramankutty, N., Reichenau, T., Schloss, A., Tian, H., Williams, L. J., and Wittenberg, U.: Carbon balance of the terrestrial biosphere in the twentieth century: analysis of CO_2, climate and land use effects with four process-based ecosystem models, Global Biogeochem. Cy., 15, 183–206, 2001.

McWilliams, D. A., Berglund, D. R., and Endres, G. J.: Soybean growth and management quick guide, North Dakota State University Extension Service, available at: http://www.ag.ndsu.edu/pubs/plantsci/rowcrops/a1174/a1174.pdf, 1999.

Title Page

Abstract | Introduction

Conclusions | References

Tables | Figures

◀ | ▶

◀ | ▶

Back | Close

Full Screen / Esc

Printer-friendly Version

Interactive Discussion

Meiyappan, P. and Jain, A. K.: Three distinct global estimates of historical land-cover change and land-use conversions for over 200 years, Front. Earth Sci., 6, 122–139, 2012.

Meyers, T. P. and Hollinger, S. E.: an assessment of storage terms in the surface energy balance of maize and soybean, Agr. Forest Meteorol., 125, 105–115, 2004.

Mitchell, K. E., Lohmann, D. L., Houser, P. R., Wood, E. F., Schaake, J. C., Robock, A., Cosgrove, B. A., Sheffield, J., Duan, Q., Luo, L., Higgins, R. W., Pinker, R. T., Tarpley, J. D., Lettenmaier, D. P., Marshall, C. H., Entin, J. K., Pan, M., Shi, W., Koren, V., Meng, J., Ramsay, B. H., and Bailey, A. A.: The multi-institution North American Land Data Assimilation System (NLDAS): utilizing multiple GCIP products and partners in a continental distributed hydrological modeling system, J. Geophys. Res., 109, D07S90, doi:10.1029/2003JD003823, 2004.

Newell, R. L. and Wilhelm, W.: Conservation tillage and irrigation effects on corn root development, Agron. J., 79, 160–165, 1987.

Norman, J. M.: Bidirectional reflectance modeling of non-homogeneous plant canopies, in: Fundamental remote sensing science research program 1985 summary report of the scene radiation and atmospheric effects characterization project, edited by Deering, D. W., NASA Technical Memorandum, Goddard Space Flight Center, Greenbelt, Maryland, 1986.

Oleson, K. W., Lawrence, D. M., Bonan, G. B., Flanner, M. G., Kluzek, E., Lawrence, P. J., Levis, S., Swenson, S. C., and Thornton, P. E.: Technical description of the community land model (CLM), NCAR Tech. Note NCAR/TN-461+STR, Natl. Cent. for Atmos. Res., Boulder, CO, 173 pp., 2004.

Oleson, K. W., Niu, G., Yang, Z., Lawrence, D. M., Thornton, P. E., Lawrence, P. J., Stöckli, R., Dickinson, R. E., Bonan, G. B., Levis, S., Dai, A., and Qian, T.: Improvements to the community land model and their impact on the hydrological cycle, J. Geophys. Res., 113, G01021, doi:10.1029/2007JG000563, 2008.

Osborne, T. M., Lawrence, D. M., Challinor, A. J., Slingo, J. M., and Wheeler, T. R.: Development and assessment of a coupled crop-climate model, Glob. Change Biol., 13, 169–183, 2007.

Penning de Vries, F. W. T., Jansen, D. M., ten Berge, H. F. M., and Bakema, A.: Simulation of ecophysiological processes of growth in several annual crops, Center for Agricultural Publishing and Documentation, Wageningen, Netherlands, 271 pp., 1989.

Rattalino Edreira, J. I. and Otegui, M. E.: Heat stress in temperate and tropical maize hybrids: Differences in crop growth, biomass partitioning and reserves use, Field Crop Res., 130, 87–89, 2012.

Sacks, W. J. and Kucharik, C. J.: Crop management and phenology trends in the US Corn Belt: impacts on yields, evapotranspiration and energy balance, Agr. Forest Meteorol., 151, 882–894, 2011.

Sakaguchi, K. and Zeng, X.: Effects of soil wetness, plant litter, and under-canopy atmospheric stability on ground evaporation in the Community Land Model (CLM3.5), J. Geophys. Res., 114, D01107, doi:10.1029/2008JD010834, 2009.

Salter, M. G., Franklin, K. A., and Whitelam, G. C.: Gating of the rapid shade-avoidance response by the circadian clock in plants, Nature, 426, 680–683, 2003.

Schenk, H. J. and Jackson, R. B.: The global biogeography of Roots, Ecol. Monogr., 72, 311–328, 2002.

Sellers, P. J.: Canopy reflectance, photosynthesis and transpiration, Int. J. Remote Sens., 6, 1335–1372, 1985.

Sellers, P. J.: Biophysical models of land surface processes, in: Climate System Modeling, edited by: Trenbern, K. E., Cambridge University Press, 1992.

Sellers, P. J., Los, S. O., Tucker, C. J., Justice, C. O., Dazlich, D. A., Collatz, G. J., and Randall, D. A.: A revised land surface parameterization (SiB2) for atmospheric GCMs. Part II: The generation of global fields of terrestrial biophysical parameters from satellite data, J. Climate, 9, 706–737, 1996a.

Sellers, P. J., Randall, D. A., Collatz, G. J., Berry, J. A., Field, C. B., Dazlich, D. A., Zhang, C., Collelo, G. D., and Bounoua, L.: A revised land surface parameterization (SiB2) for atmospheric GCMs. Part I: model formulation, J. Climate, 9, 676–705, 1996b.

Shaw, R. H.: Climate requirement, in: Corn and Corn Improvement, edited by: Sprague, G. F. and Dudley, J. W., American Society of Agronomy, Madison, WI, 609–638, 1988.

Sitch, S., Smith, B., Prentice, I. C., Arneth, A., Bondeau, A., Cramer, W., Kaplans, J. O., Levis, S., Lucht, W., Sykes, M. T., Thonicke, K., and Venevsky, S.: Evalution of ecosystem dynamics, plant geography and terrestrial carbon cycling in the LPJ dynamic global vegetation model, Global Change Biol., 9, 161–185, 2003.

Sitch, S., Brovkin, V., von Bloh, W., van Vuuren, D., Eickhout, B., and Ganopolski, A.: Impacts of future land cover changes on atmospheric CO_2 and climate, Global Biogeochem. Cy., 19, GB2013, doi:10.1029/2004GB002311, 2005.

Smith, E. W., Tolbert, N. E., and Ku, H.: Variables affecting the CO_2 compensation point, Plant Physiol., 58, 143–146, 1976.

Implementation of dynamic crop growth processes into a land surface model

Y. Song et al.

Title Page

Abstract	Introduction
Conclusions	References
Tables	Figures

◀◀ ▶▶

◀ ▶

Back Close

Full Screen / Esc

Printer-friendly Version

Interactive Discussion

Suyker, A. E. and Verma, S. B.: Evapotranspiration of irrigated and rainfed maize-soybean cropping systems, Agr. Forest. Meteorol., 149, 443–452, 2009.

Suyker, A. E. and Verma, S. B.: Coupling of carbon dioxide and water vapor exchanges of irrigated and rainfed maize-soybean cropping systems and water productivity, Agr. Forest. Meteorol., 150, 553–563, 2010.

Suyker, A. E., Verma, S. B., Burba, G. G., Arkebauer, T. J., Walters, D. T., and Hubbard, K. G.: Growing season carbon dioxide exchange in irrigated and rainfed maize, Agr. Forest Meteorol., 124, 1–13, 2004.

Tsvetsinskaya, E. A., Mearns, L. O., and Easterling, W. E.: Investigating the effect of seasonal plant growth and development in three-dimensional atmospheric simulations. Part I: Simulation of surface fluxes over the growing season, J. Climate, 14, 692–709, 2001.

Twine, T. E., Kustas, W. P., Norman, J. M., Cook, D. R., Houser, P. R., Meyers, T. P., Prueger, J. H., Starks, P. J., and Wesely, M. L.: Correcting eddy-covariance flux underestimates over a grassland, Agr. Forest Meteorol., 103, 279–300, 2000.

USDA-NASS: National crop progess-terms and definitions, USDA-NASS, Washington, DC, available at: http://www.nass.usda.gov/Publications/National_Crop_Progress/Terms_and_Definitions/index.asp, 2009.

USDA-OCE, Weekly weather and crop bulletin, USDA-OCE, Washington, DC, available at: http://www.usda.gov/oce/weather/pubs/Weekly/Wwcb/index.htm, 2010.

Urban, D., Roberts, M. J., Schlenker, W., and Lobell, D. B.: Projected temperature changes indicate significant increase in interannual variability of US maize yields, Climatic Change, 112, 525–533, 2012.

Van den Hoof, C., Hanert, E., and Vidale, P. L.: Simulation dynamic crop growth with an adapted land surface model-JULES-SUCROS: model development and validation, Agr. Forest Meteorol., 151, 137–153, 2011.

Williams, M., Richardson, A. D., Reichstein, M., Stoy, P. C., Peylin, P., Verbeeck, H., Carvalhais, N., Jung, M., Hollinger, D. Y., Kattge, J., Leuning, R., Luo, Y., Tomelleri, E., Trudinger, C. M., and Wang, Y.-P.: Improving land surface models with FLUXNET data, Biogeosciences, 6, 1341–1359, doi:10.5194/bg-6-1341-2009, 2009.

Willmott, C. J.: On the validation of models, Phys. Geogr., 2, 184–194, 1981.

Willmott, C. J., Robeson, S. M., and Matsuura, K.: A refined index of model performance, Int. J. Climateol., 32, 2088–2094, 2012.

Wilson, K. B., Goldstein, A. H., Falge, E., Aubinet, M., Baldocchi, D., Berbingier, P., Bernhofer, C., Ceulemans, R., Dolman, H., Field, C., Grelle, A., Law, B., Meyers, T., Moncrieff, J., Monson, R., Oechel, W., Tenhunen, J., Valentini, R., and Verma, S.: Energy balance closure at FLUXNET sites, Agr. Forest Meteorol., 113, 223–243, 2002.

5 Wingeyer, A. B.: The effect of residue C:N ratio on the turnover of N and C in various soil organic matter fractions, M. S. thesis, The Graduate College at the University of Nebraska, Lincoln, Nebraska, 65 pp., 2007.

Winstanley, D.: Illinois water and climate summary July 2003, Illinois State Water Survey, Champaign, IL, 2003.

10 Yang, X., Witting, V., Jain., A. K., and Post, W. M.: Integration of nitrogen cycle dynamics into the Integrated Science Assessment Model for the study of terrestrial ecosystem responses to global change, Global Biogeochem. Cy., 23, GB4029, doi:10.1029/2009GB003474, 2009.

Verma, S. B., Dobermann, A., Cassman, K. G., Walters, D. T., Knops, J. M., Arkebauer, T. J., Suyker, A. E., Burba, G. G., Amos, B., Yang, H., Ginting, D., Hubbard, K. G., Gitelson, A. A.,

15 and Walter-Shea, E. A.: Annual carbon dioxide exchange in irrigated and rainfed maize-based agroecosystems, Agr. Forest Meteorol., 131, 77–96, 2005.

Zeng, X. and Decker, M.: Improving the numerical solution of soil moisture-based Richards equation for land models with a deep or shallow water table, J. Hydrometeorol., 10, 308–319, 2009.

20 Zeng, X. and Wang, A.: Consistent parameterization of roughness length and displacement height for sparse and dense canopies in land models, J. Hydrometeorol., 8, 730–737, 2007.

Zeng, X., Shaikh, M., Dai, Y., Dickinson, R. E., and Myneni, R.: Coupling of the Common Land Model to the NCAR Community Climate Model, J. Climate, 15, 1832–1854, 2002.

Table 1. The estimated Willmott index to quantify the degree to which observed hourly GPP, energy and water fluxes are captured by the model for corn and soybean at Mead and Bondville site. The dr_h is Willmott index for hourly observed data and model results and dr_d is index for daily mean observed data and model results. The n is the number of observation samples.

Data	Sites	Crop	n	dr_h	dr_d
GPP	Mead, NE	Corn	5640	0.86	0.86
		Soybean	5568	0.85	0.83
	Bondville, IL	Corn	5564	0.82	0.71
		Soybean	4968	0.86	0.92
Rn	Mead, NE	Corn	5640	0.87	0.89
		Soybean	5568	0.86	0.90
	Bondville, IL	Corn	5664	0.91	0.83
		Soybean	4632	0.91	0.93
H	Mead, NE	Corn	5640	0.68	0.71
		Soybean	5568	0.68	0.68
	Bondville, IL	Corn	4281	0.60	0.47
		Soybean	3249	0.69	0.77
LH	Mead, NE	Corn	5640	0.86	0.87
		Soybean	5568	0.84	0.77
	Bondville, IL	Corn	4281	0.83	0.50
		Soybean	3249	0.84	0.88

Table 2. The estimated Willmott index to quantify the degree to which observed GPP and LH are captured by the model with (ISAM-DynamicR) and without (ISAM-StaticR) dynamic carbon allocation and root distribution schemes under corn and soybean at Mead and Bondville sites. The dr_h is Willmott index for hourly observed data and model results and dr_d is index for daily mean observed data and model results. The n is the number of observation samples.

Data	Sites	Crop	n	dr_h (ISAM-StaticR)	dr_h (ISAM-DynamicR)	dr_d (ISAM-StaticR)	dr_d (ISAM-DynamicR)
GPP	Mead, NE	Corn	5640	0.78	0.86	0.57	0.86
		Soybean	5568	0.82	0.85	0.72	0.83
	Bondville, IL	Corn	5564	0.82	0.82	0.71	0.71
		Soybean	4968	0.85	0.86	0.81	0.92
LH	Mead, NE	Corn	5640	0.79	0.86	0.55	0.87
		Soybean	5568	0.81	0.84	0.64	0.77
	Bondville, IL	Corn	4281	0.82	0.83	0.40	0.50
		Soybean	3249	0.82	0.84	0.64	0.88

Table A1. Variables and parameters that appear in the model equations.

Symbol	Definition	Value	Source
V_{cmax25}	Maximum carboxylation rate at the reference temperature of 25 °C	54 100 μmol m^{-2} s^{-1}	Collatz et al. (1992); Bernacchi et al. (2005)
m	The slope of regression carbon assimilation to stomatal conductance in Ball-Berry equation	3.9	Collatz et al. (1992)
b	Minimum stomatal conductance in Ball-Berry equation	0.04, 0.01 [mol m^{-2} s^{-1}]	Collatz et al. (1992)
T_{high}	1/2 point of high temperature inhibition function for carbon assimilation	318, 313 [K]	Dai et al. (2003) Hofstra and Hesketh (1969)
T_{low}	1/2 point of low temperature inhibition for carbon assimilation	283, 283 [K]	Dai et al. (2003) Hofstra and Hesketh 1969
S_{low}	Slope of low temperature inhibition function for carbon assimilation	0.3, 0.3 [K^{-1}]	Dai et al. (2003) Hofstra and Hesketh (1969)
S_{high}	Slope of high temperature inhibition function for carbon assimilation	0.2, 0.2 [K^{-1}]	Dai et al. (2003) Hofstra and Hesketh (1969)
χ_{leaf}	Leaf angle distribution parameter in two-stream approximation	0, 0	Sheller (1985); Norman (1986)
R_{11}	Reflection fraction of green leaves to visible radiation	0.11, 0.11	Sheller (1985); Norman (1986)
R_{12}	Reflection fraction of green leaves to near-infrared radiation	0.58, 0.52	Sheller (1985); Norman (1986)
R_{21}	Reflection fraction of dead leaves to visible radiation	0.36, 0.31	Sheller (1985); Norman (1986)
R_{22}	Reflection fraction of dead leaves to near-infrared radiation	0.58, 0.58	Sheller (1985); Norman (1986)
τ_{11}	Transmittance fraction of green leaves to visible radiation	0.07, 0.04	Sheller (1985); Norman (1986)
τ_{12}	Transmittance fraction of green leaves to near-infrared radiation	0.25, 0.32	Sheller (1985); Norman (1986)
τ_{21}	Transmittance fraction of dead leaves to visible radiation	0.22, 0.36	Sheller (1985); Norman (1986)
τ_{22}	Transmittance fraction of dead leaves to near-infrared radiation	0.38, 0.38	Sheller (1985); Norman (1986)
T_{base}	Base atmospheric temperature for crop planting and growth in Eqs. (A1–2)	283, 283 [K]	Darby and Lauer (2000);
$T{soil}_{critical}$	Base soil temperature for crop planting in Eq. (A1)	285, 285 [K]	Penning de Vries et al. (1989)
T_{mean_i}	Daily mean atmospheric temperature of the i day	Varies	
$Tsoil_{mean\_i}$	Daily mean soil temperature of the i day	Varies	
$GDD0_{min}$	Minimum running accumulation of growing degree days above 0 °C for planting	170, 210 [°]	This study
GDD_{max}	Required total heat above base temperature for mature	1620, 1670 [°C]	This study
HUI_i	Heat unit index of the i day	Varies	
HUI_{v1}	Minimum heat unit index during the initial vegetative period	0.10, 0.15	Darby and Lauer (2000); McWilliams et al. (2004); USDA-NASS (2009); USDA-OCE(2010); This study
HUI_{v2}	Minimum heat unit index during the normal vegetative period	0.19, 0.17	
HUI_{r1}	Minimum heat unit index during the initial reproductive period	0.63, 0.69	
HUI_{r2}	Minimum heat unit index during the post reproductive period	0.80, 0.85	
HUI_{v2m}	Heat unit index in Eq. (A19)	0.38, 0.20	
HUI_{r1m}	Heat unit index in Eq. (A20)	0.69, 0.79	
D_e	Total days during the emergence period	22, 22	
D_{v1}	Total days during the initial vegetative period	17, 17	
D_{v2}	Total days during the normal vegetative period	51, 53	
D_{r1}	Total days during the initial reproductive period	37, 28	
D_{r2}	Total days during the post reproductive period	32, 30	

Table A1. Continued.

Symbol	Definition	Value	Source
D_{plant}	Julian day of planting time	Varies	
$D_{first_{v1}}$	Julian day of the first day of the initial vegetative period	Varies	
$D_{first_{v2}}$	Julian day of the first day of the normal vegetative period	Varies	
$D_{first_{r1}}$	Julian day of the first day of the initial reproductive period	Varies	
$D_{first_{r2}}$	Julian day of the first day of the post reproductive period	Varies	
D_i	Julian day of the i day	Varies	
$C_{storage}$	Initial carbon storage in seed during the emergence	Constant	Input parameter
$C_{storage\_ref}$	Initial carbon storage in seed as referenced seeding rate	20, 30 [g C]	This study
R_{seed}	Seeding rate	Constant	Input parameter
R_{seed_ref}	Referenced seeding rate	62 236, 370 644	
GPP_i	Gross primary productivity on the i day	Varies	
NPP_i	Net primary productivity on the i day	Varies	
Rn	Net solar radiation	Varies	
H	Canopy sensible heat	Varies	
LH	Canopy latent heat	Varies	
$C_{g\_leaf_i}$	Green leaf carbon on the i day	Varies	
$C_{d\_leaf_i}$	Dead leaf carbon on the i day	Varies	
C_{stem_i}	Stem carbon on the i day	Varies	
C_{root_i}	Root carbon on the i day	Varies	
$R_{m\_leaf_i}$	Maintenance respiration of leaf	Varies	
$R_{m\_stem_i}$	Maintenance respiration of stem	Varies	
$R_{m\_root_i}$	Maintenance respiration of root	Varies	
$R_{m\_grain_i}$	Maintenance respiration of grain	Varies	
R_{g_i}	Total growth respiration on the i day	Varies	
$R_{g\_leaf_i}$	Leaf growth respiration on the i day	Varies	
$R_{g\_stem_i}$	Stem growth respiration on the i day	Varies	
$R_{g\_root_i}$	Root growth respiration on the i day	Varies	
$R_{g\_grain_i}$	Grain growth respiration on the i day	Varies	
k_{leaf}	Maintenance respiration coefficients of leaf at 20 °C	3.37×10^{-7} [g C g N^{-1} s^{-1}]	Penning De Vries et al. (1989)
k_{stem}	Maintenance respiration coefficients of stem at 20 °C	1.05×10^{-7} [g C g N^{-1} s^{-1}]	Penning De Vries et al. (1989)
k_{root}	Maintenance respiration coefficients of root at 20 °C	3.37×10^{-7} [g C g N^{-1} s^{-1}]	Penning De Vries et al. (1989)
k_{grain}	Maintenance respiration coefficients of grain at 20 °C	1.68×10^{-7} [g C g N^{-1} s^{-1}]	Penning De Vries et al. (1989)
CN_{leaf}	C : N ratio of leaf	32, 12	Wingeyer (2007)
CN_{stem}	C : N ratio of stem	33, 12	Wingeyer (2007)
CN_{root}	C : N ratio of root	48, 50	Wingeyer (2007)
CN_{grain}	C : N ratio of grain	200, 200	Wingeyer (2007)
T_{leaf}	Leaf temperature per time step	Varies	
T_{soil}	Soil temperature per time step	Varies	
Al_0	Allocation fraction for leaf carbon during the initial vegetative period	0.5, 0.3	This study
As_0	Allocation fraction for stem carbon during the initial vegetative period	0.2, 0.32	This study
Ar_0	Allocation fraction for root carbon during the initial vegetative period	0.3, 0.38	This study
Al_{r1}	Initial allocation fraction for leaf carbon during the initial reproductive period	0, 0	This study
As_{r1}	Initial allocation fraction for stem carbon during the initial reproductive period	0.45, 0.35	This study
Ar_{r1}	Initial allocation fraction for root carbon during the initial reproductive period	0.10, 0.20	This study
Ag_{r1}	Initial allocation fraction for grain carbon during the initial reproductive period	0.45, 0.45	This study
Al_{r2}	Initial allocation fraction for leaf carbon during the post reproductive period	0, 0	This study
As_{r2}	Initial allocation fraction for stem carbon during the post reproductive period	0, 0	This study
Ar_{r2}	Initial allocation fraction for root carbon during the post reproductive period	0.45, 0.65	This study
Ag_{r2}	Initial allocation fraction for grain carbon during the post reproductive period	0.55, 0.35	This study
Al_{v2m}	Allocation fraction for leaf in Eq. (A19)	0.79, 0.85	This study
As_{v2m}	Allocation fraction for stem in Eq. (A19)	0.10, 0.12	This study
Ar_{v2m}	Allocation fraction for root in Eq. (A19)	0.11, 0.03	This study

Title Page

Abstract | Introduction

Conclusions | References

Tables | Figures

|◄ | ►|

◄ | ►

Back | Close

Full Screen / Esc

Printer-friendly Version

Interactive Discussion

Table A1. Continued.

Symbol	Definition	Value	Source
$k1_{v2}$	Increasing rate of leaf allocation fraction with HUI in Eq. (A19)	1.0, 9.5	This study
$k2_{v2}$	Increasing rate of stem allocation fraction with HUI in Eq. (A19)	2.4, 0.0	This study
$k1_{r1}$	Increasing rate of grain allocation fraction with HUI in Eq. (A20)	1.0, 2.1	This study
Al	Allocation fraction for leaf on each day	Varies	
As	Allocation fraction for stem on each day	Varies	
Ar	Allocation fraction for root on each day	Varies	
Ag	Allocation fraction for grain on each day	Varies	
ω	Sensitivity parameter of allocation to changes in availability of light, water and N in Eq. (A22)	0.8	Arora and Boer (2005)
LS_i	Scalar index of the availability of light in Eq. (A22)	Varies	
WS_i	Scalar index of availability of water in Eq. (A22)	Varies	
NS_i	Scalar index of availability of N in Eq. (A22)	Varies	Yang et al. (2009)
K_n	Light extinction coefficient in Eq. (A23)	−0.5	Arora and Boer (2005)
w_i	Crop wilting factor for soil layer i in Eq. (A24)	Varies	
$\theta_{sat,i}$	The saturation water content for soil layer i	Function of soil texture	Oleson et al. (2008)
$\theta_{ice,i}$	The volumetric ice content for soil layer i	Varies	
$\theta_{liq,i}$	The volumetric liquid water content for soil layer i	Varies	
ψ_{close}	The water potential at full stomatal closure	−275 000 mm	Oleson et al. (2008)
ψ_{open}	The water potential at full stomatal open	−74 000 mm	Oleson et al. (2008)
ψ_i	The soil water matric potential for soil layer i	Varies	
Rl	Dead rate of green leaves	Varies	
Rn_d	Dead rate of green leaves due to aging	Varies	
Rt_d	Dead rate of green leaves due to cold temperature	Varies	
Rw_d	Dead rate of green leaves due to drought	Varies	
TS_i	Scalar index of cold temperature stress in Eq. (A28)	Varies	
Rt_{max}	Maximum death rate of green leaves due to cold temperature	0.30	This study
Rw_{max}	Maximum death rate of green leaves due to drought	0.03	This study
T_{cold}	Cold temperature threshold for cold-induced death of green leaves	285 [K]	This study
kl_1	Remove fraction of previous produced leaf litter	1.0	This study
kl_2	Remove fraction of new produced leaf litter	0.77	This study
rlt_{leaf}	Leaf turnover rate	1.21, 1.47 [yr]	This study
rlt_{stem}	Stem turnover rate	1.0 [yr]	This study
rlt_{root}	Root turnover rate	1.0 [yr]	This study
$L_{d\_leaf_i}$	Leaf litter carbon on i day	Varies	
L_{stem_i}	Stem litter carbon on i day	Varies	
L_{root_i}	Root litter carbon on i day	Varies	
ϵ	Parameter in Eq. (A31)	0.04	Arora and Boer (2005)
κ	Parameter in Eq. (A31)	1.6	Arora and Boer (2005)
RS_{min}	Minimum root: shoot ratio of crop	0.07	Arora and Boer (2005)
LAI	Leaf area index	Varies	
LAI_d	Dead leaf area index	Varies	
LAI_g	Green leaf area index	Varies	
LAI_{max}	Maximum leaf area index	6.0, 6.0 [m^2 m^{-2}]	Verma et al. (2005)
SLA	Specific leaf area	0.04, 0.05 [m^2 g^{-1}]	Calculation based on AmeriFlux data
H_a	Maximum canopy height	2.3, 0.9 [m]	AmeriFlux data
H_i	Canopy height on the i day	Varies	
B_{leaf_i}	Leaf biomass on i day	Varies	
B_{stem_i}	Stem biomass on i day	Varies	
B_{root_i}	Root biomass on i day	Varies	
D_{root_i}	Root depth on i day	Varies	
zi(j)	The depth of soil layer j	Constant	
f_j	Accumulated root fraction in soil layer j	Varies	
r_j	Root fraction in soil layer j	Varies	
L_{max}	The soil layer where root tip located	Varies	
α	Root growth direction parameter in Eqs. (A41–42)	0.7	Calibration based on Newell (1987)
bb	Variable root distribution parameter in Eqs. (A41–42)	0.53	Calibration based on Newell (1987)

Table A2. ISAM model equations in this study.

Function		Equations
Phenology	For planting date (D_{plant})	Eq. (A1)
	$\begin{cases} \dfrac{\sum\limits_{i=D_i-6}^{i=D_i} T_{mean\_i}}{7} > T_{base} \\ \dfrac{\sum\limits_{i=D_i-6}^{i=D_i} T soil_{mean\_i}}{7} > Tsoil_{critical} \\ \sum\limits_{i=1}^{i=D_i} (T_{mean\_i} - 273.16) > GDD0_{min} \end{cases}$	
Phenology	For heat unit index	Eq. (A2)
	$HUI_i = \dfrac{\sum\limits_{i=D_{plant}}^{i=D_i} (T_{mean\_i} - T_{base})}{GDD_{max}}$	
Phenology	For emergence period	Eq. (A3)
	$\begin{cases} 0 \le HUI_i \le HUI_{v1} \\ (D_i - D_{plant} + 1) \le D_e \\ LAI_i \le LAI_{max} \end{cases}$	
Phenology	For initial vegetative period	Eq. (A4)
	$\begin{cases} HUI_{v1} < HUI_i \le HUI_{v2} \\ (D_i - D_{first_{v1}} + 1) \le D_{v1} \\ LAI_i \le LAI_{max} \end{cases}$	
Phenology	For normal vegetative period	Eq. (A5)
	$\begin{cases} HUI_{v2} < HUI_i \le HUI_{r1} \\ (D_i - D_{first_{v2}} + 1) \le D_{v2} \\ LAI_i \le LAI_{max} \end{cases}$	

Table A2. Continued.

Function		Equations
Phenology	For initial reproductive period $\begin{cases} \text{HUI}_{r1} < \text{HUI}_i \leq \text{HUI}_{r2} \\ (D_i - D_{\text{first}_{r1}} + 1) \leq D_{r1} \end{cases}$	Eq. (A6)
Phenology	For post reproductive period $\begin{cases} \text{HUI}_{r2} < \text{HUI}_i \leq 1.0 \\ (D_i - D_{\text{first}_{r2}} + 1) \leq D_{r2} \end{cases}$	Eq. (A7)
Phenology	Cold destroy on yield is induced by $\sum_{i=D_{i-4}}^{i=D_i} T_{\text{mean}\_i} < 273.16$	Eq. (A8)
Phenology	Silk delay is induced by $\begin{cases} \sum_{i=D_{i-2}}^{i=D_i} T_{\text{mean}_i} > 303.16 \\ \sum_{i=D_{i-2}}^{i=D_i} \text{WS}_i < 0.5 \end{cases}$	Eq. (A9)
Carbon allocation	For initial carbon during the emergence period $C_{\text{storage}} = C_{\text{storage\_ref}} * R_{\text{seed}} / R_{\text{seed\_ref}}$	Eq. (A10)
Carbon allocation	Foe carbon allocation during the emergence period $\begin{cases} C_{g\_\text{leaf}_i} = 0.6 * \dfrac{C_{\text{storage}} * \text{HUI}_i}{\text{HUI}_{v1}} \\ C_{\text{root}_i} = 0.4 * \dfrac{C_{\text{storage}} * \text{HUI}_i}{\text{HUI}_{v1}} \end{cases}$	Eq. (A11)
Carbon allocation	For daily net primary production $\text{NPP}_i = \text{GPP}_i - (R_{m\_\text{leaf}_i} + R_{m\_\text{stem}_i} + R_{m\_\text{root}_i} + R_{m\_\text{grain}_i}) - R_{g_i}$	Eq. (A12)

Table A2. Continued.

Function		Equations
Carbon allocation	For maintenance respiration $$\begin{cases} R_{m\_leaf_i} = k_{leaf} * \frac{C_{g\_leaf_i} + C_{d\_leaf_i}}{CN_{leaf}} * g(T_{leaf}) \\ R_{m\_stem_i} = k_{stem} * \frac{C_{stem}}{CN_{stem}} * g(T_{leaf}) \\ R_{m\_root_i} = k_{root} * \frac{C_{root}}{CN_{root}} * g(T_{soil}) \\ R_{m\_grain_i} = k_{grain} * \frac{C_{grain}}{CN_{grain}} * g(T_{leaf}) \end{cases}$$	Eq. (A13)
Carbon allocation	Q_{10} temperature function for maintenance respiration $$\begin{cases} g(T_{leaf}) = Q_{10\_above}^{(T_{leaf} - 293.16)} \\ g(T_{soil}) = Q_{10\_below}^{(T_{soil} - 293.16)} \end{cases}$$	Eq. (A14)
Carbon allocation	Temperature adjusted Q_{10} value $$\begin{cases} Q_{10\_above} = 3.22 - 0.046 * (T_{leaf} - 273.16) \\ Q_{10\_below} = 3.22 - 0.046 * (T_{soil} - 273.16) \end{cases}$$	Eq. (A15)
Carbon allocation	For growth respiration $$R_{g_i} = \max\left(0, 0.25 * \left(GPP - R_{m_{leaf_i}} - R_{m_{stem_i}} - R_{m_{root_i}} - R_{m_{grain_i}}\right)\right)$$	Eq. (A16)

Table A2. Continued.

Function		Equations
Carbon allocation	Partitioning of the growth respiration into each vegetation pool	Eq. (A17)

$$\begin{cases} R_{g_{\text{leaf}_i}} = R_{g_i} * \dfrac{C_{g_{\text{leaf}_i}} + C_{d_{\text{leaf}_i}}}{C_{g_{\text{leaf}_i}} + C_{d\_\text{leaf}_i} + C_{\text{stem}_i} + C_{\text{root}_i} + C_{\text{grain}_i}} \\[2ex] R_{g_{\text{stem}_i}} = R_{g_i} * \dfrac{C_{\text{stem}_i}}{C_{g_{\text{leaf}_i}} + C_{d\_\text{leaf}_i} + C_{\text{stem}_i} + C_{\text{root}_i} + C_{\text{grain}_i}} \\[2ex] R_{g_{\text{root}_i}} = R_{g_i} * \dfrac{C_{\text{root}_i}}{C_{g_{\text{leaf}_i}} + C_{d\_\text{leaf}_i} + C_{\text{stem}_i} + C_{\text{root}_i} + C_{\text{grain}_i}} \\[2ex] R_{g_{\text{grain}_i}} = R_{g_i} * \dfrac{C_{\text{grain}_i}}{C_{g_{\text{leaf}_i}} + C_{d\_\text{leaf}_i} + C_{\text{stem}_i} + C_{\text{root}_i} + C_{\text{grain}_i}} \end{cases}$$

Function		Equations
Carbon allocation	Thermal determined carbon allocation factor for initial vegetative period	Eq. (A18)

$$\begin{cases} Al = Al_0 \\ As = As_0 \\ Ar = Ar_0 \\ Ag = Ag_0 \end{cases}$$

Function		Equations
Carbon allocation	Thermal determined carbon allocation factor for normal vegetative period	Eq. (A19)

When $\text{HUI}_i \leq \text{HUI}_{v2m}$

$$\begin{cases} Al = Al_0 + (\text{HUI}_i - \text{HUI}_{v1}) * k1_{v2} \\ As = As_0 \\ Ar = Ar_0 - (\text{HUI}_i - \text{HUI}_{v1}) * k1_{v2} \\ Ag = 0 \end{cases}$$

When $\text{HUI}_i > \text{HUI}_{v2m}$

$$\begin{cases} Al = Al_{v2m} - (\text{HUI}_i - \text{HUI}_{v2m}) * k2_{v2} \\ As = As_{v2m} + (\text{HUI}_i - \text{HUI}_{v2m}) * k2_{v2} \\ Ar = Ar_{v2m} \\ Ag = 0 \end{cases}$$

Table A2. Continued.

Function		Equations
Carbon allocation	Thermal determined carbon allocation factor for initial reproductive period When $HUI_i \leq HUI_{r1m}$ $\begin{cases} Al = Al_{r1} \\ As = As_{r1} \\ Ar = Ar_{r1} \\ Ag = Ag_{r1} \end{cases}$ When $HUI_i > HUI_{r1m}$ $\begin{cases} Al = Al_{r1} \\ As = As_{r1} - (HUI_i - HUI_{r1m}) * k1_{r1} \\ Ar = Ar_{r1} \\ Ag = Ag_{r1} + (HUI_i - HUI_{r1m}) * k1_{r1} \end{cases}$	Eq. (A20)
Carbon allocation	Thermal determined carbon allocation factor for post reproductive period $\begin{cases} Al = Al_{r2} \\ As = As_{r2} \\ Ar = Ar_{r2} \\ Ag = Ag_{r2} \end{cases}$	Eq. (A21)
Carbon allocation	Dynamic carbon allocation factor function $\begin{cases} As = \dfrac{As + \omega * (1 - LS_i)}{1 + \omega * (3 - LS_i - WS_i - NS_i)} \\ Ar = \dfrac{Ar + \omega * (2 - WS_i - NS_i)}{1 + \omega * (3 - LS_i - WS_i - NS_i)} \\ Al = \dfrac{Al}{1 + \omega * (3 - LS_i - WS_i - NS_i)} \end{cases}$	Eq. (A22)
Carbon allocation	Light availability factor in dynamic carbon allocation factor function $LS_i = e^{(-K_n * LAI_i)}$	Eq. (A23)

Table A2. Continued.

Function		Equations
Carbon allocation	Water availability factor in dynamic carbon allocation factor function $$\begin{cases} \mathrm{WS}_i = \sum_{i=1}^{i=10} w_i * r_i \\ w_i = \begin{cases} \left(\frac{\theta_{\mathrm{sat},i} - \theta_{\mathrm{ice},i}}{\theta_{\mathrm{sat},i}} \right) \left(\frac{\psi_i - \psi_{\mathrm{close}}}{\psi_{\mathrm{open}} - \psi_{\mathrm{close}}} \right) \leq 1 & \theta_{\mathrm{liq},i} > 0 \\ 0 & \theta_{\mathrm{liq},i} = 0 \end{cases} \end{cases}$$	Eq. (A24)
Carbon allocation	For carbon allocation during initial and normal vegetative period $$\begin{cases} C_{g\_\mathrm{leaf}_i} = C_{g\_\mathrm{leaf}_{i-1}} + \mathrm{NPP} * \mathrm{Al} \\ C_{d_{\mathrm{leaf}_i}} = 0 \\ C_{\mathrm{stem}_i} = C_{\mathrm{stem}_{i-1}} + \mathrm{NPP} * \mathrm{As} \\ C_{\mathrm{root}_i} = C_{\mathrm{root}_{i-1}} + \mathrm{NPP} * \mathrm{Ar} \\ C_{\mathrm{grain}_i} = C_{\mathrm{grain}_{i-1}} + \mathrm{NPP} * \mathrm{Ag} \end{cases}$$	Eq. (A25)
Carbon allocation	For carbon allocation during initial and post reproductive period When NPP > 0 $$\begin{cases} C_{g\_\mathrm{leaf}_i} = \max\left(0, \left(C_{g\_\mathrm{leaf}_i} - R_{m_{\mathrm{leaf}}} - C_{g\_\mathrm{leaf}_i} * \mathrm{Rl} \right) \right) \\ C_{d\_\mathrm{leaf}_i} = (C_{d\_\mathrm{leaf}_{i-1}} + C_{g\_\mathrm{leaf}_i}) * \mathrm{Rl} \\ C_{\mathrm{stem}_i} = C_{\mathrm{stem}_{i-1}} + \mathrm{NPP} * \mathrm{As} \\ C_{\mathrm{root}_i} = C_{\mathrm{root}_{i-1}} + \mathrm{NPP} * \mathrm{Ar} \\ C_{g\mathrm{rain}_i} = C_{\mathrm{grain}_{i-1}} + \mathrm{NPP} * \mathrm{Ag} \end{cases}$$ When NPP ≤ 0 $$\begin{cases} C_{g\_\mathrm{leaf}_i} = \max\left(0, \left(C_{g\_\mathrm{leaf}_i} - R_{m_{\mathrm{leaf}}} - C_{g\_\mathrm{leaf}_i} * \mathrm{Rl} \right) \right) \\ C_{d\_\mathrm{leaf}_i} = C_{d\_\mathrm{leaf}_{i-1}} + C_{g\_\mathrm{leaf}_i} * \mathrm{Rl} \\ C_{\mathrm{stem}_i} = C_{\mathrm{stem}_{i-1}} - C_{\mathrm{stem}_{i-1}} * 0.05 * \mathrm{WS}_i \\ C_{\mathrm{root}_i} = C_{\mathrm{root}_{i-1}} - C_{\mathrm{root}_{i-1}} * 0.05 * \mathrm{WS}_i \\ C_{\mathrm{grain}_i} = C_{\mathrm{grain}_{i-1}} + C_{\mathrm{stem}_{i-1}} * 0.05 * \mathrm{WS}_i + C_{\mathrm{root}_{i-1}} * 0.05 * \mathrm{WS}_i \end{cases}$$	Eq. (A26)

Table A2. Continued.

Function		Equations
Carbon allocation	Death rate of green leaves $Rl = Rn_d + Rt_d + Rw_d$	Eq. (A27)
Carbon allocation	Each death rate of green leaves due to aging, cold temperature and drought $\begin{cases} Rn_d = 1/(rlt_{leaf}*365) \\ Rt_d = Rt_{max}*(1 - TS_i)^{3.0} \\ Rw_d = Rw_{max}*(1 - WS_i)^{3.0} \end{cases}$	Eq. (A28)
Carbon allocation	Temperature stress parameters for green leaves death $TS_i = \begin{cases} 1 & T_{mean\_i} > T_{cold} \\ \frac{(T_{mean\_i} - T_{cold} - 5.0)}{5.0} & T_{cold} > T_{mean\_i} > (T_{cold} - 5.0) \\ 0 & T_{mean\_i} \leq (T_{cold} - 5.0) \end{cases}$	Eq. (A29)
Carbon allocation	Turnover rate of green rate due to aging $rlt_{leaf} = \left(\frac{0.025}{SLA}\right)^2$	Eq. (A30)
Carbon allocation	Structure limitation function 1 for carbon $\left(C_{stem_i} + C_{root_i}\right) = e*C_{leaf_i}^{k}$	Eq. (A31)
Carbon allocation	Structure limitation function 2 for carbon allocation $\frac{C_{root_i}}{C_{leaf_i} + C_{stem_i} + C_{grain_i}} \geq RS_{min}$	Eq. (A32)
Litter Production	Litter production for stem $L_{stem_i} = C_{stem_i}/(rlt_{stem}*365)$	Eq. (A33)

Table A2. Continued.

Function		Equations
Litter Production	Litter production for root $L_{\text{root}_i} = C_{\text{root}_i}/(\text{rlt}_{\text{root}}*365)$	Eq. (A34)
Litter Production	Litter production for dead leaves $L_{d\_\text{leaf}_i} = C_{d\_\text{leaf}_{i-1}}*\text{kl}_1 + (C_{d\_\text{leaf}_i} - C_{d\_\text{leaf}_{i-1}})*\text{kl}_2$	Eq. (A35)
LAI	For total LAI $\text{LAI} = (C_{g\_\text{leaf}_i} + C_{d\_\text{leaf}_i})*\text{SLA}$	Eq. (A36)
LAI	For dead LAI $\text{LAI}_d = C_{d\_\text{leaf}_i}*\text{SLA}$	Eq. (A37)
LAI	For green LAI $\text{LAI}_g = \max(0., (\text{LAI} - \text{LAI}_g))$	Eq. (A38)
Canopy Height	For canopy height $\begin{cases} B_{\text{leaf}_i} = 0.1*(C_{g\_\text{leaf}_i} + C_{d\_\text{leaf}_i})*(\frac{1}{\text{CN}_{\text{leaf}}} + 1) \\ B_{\text{stem}_i} = 0.1*C_{\text{stem}_i}*(\frac{1}{\text{CN}_{\text{stem}}} + 1) \\ H_{\text{ci}} = H_a*(B_{\text{leaf}_i} + B_{\text{stem}_i})^{0.385} \end{cases}$	Eq. (A39)
Root depth and distribution	For root biomass $B_{\text{root}_i} = 0.1*C_{\text{root}_i}*\left(\frac{1}{\text{CN}_{\text{root}}} + 1\right)$	Eq. (A40)
Root depth and distribution	For root depth $D_{\text{root}_i} = \frac{3*(B_{\text{root}_i})^{\alpha}}{\text{bb}}$	Eq. (A41)

Table A2. Continued.

Function		Equations
Root depth and distribution	Accumulated root fraction in each soil layer (j) $$f_j = \begin{cases} \left(1 - e^{\frac{(-bb*zi(j))}{(D_{root_i})^\alpha}}\right) & zi(j) \le D_{root_i} \\ \left\{\left(1 - e^{\frac{(-bb*D_{root_i})}{(B_{root_i})^\alpha}}\right)\right. \\ \left. L_{max} = j \right. & zi(j) > D_{root_i} \end{cases}$$	Eq. (A42)
Root depth and distribution	Root fraction in each soil layer (j) $$r_j = \begin{cases} f_j & j = 1 \\ f_j - f_{j-1} & 2 \le j \le L_{max} \end{cases}$$	Eq. (A43)
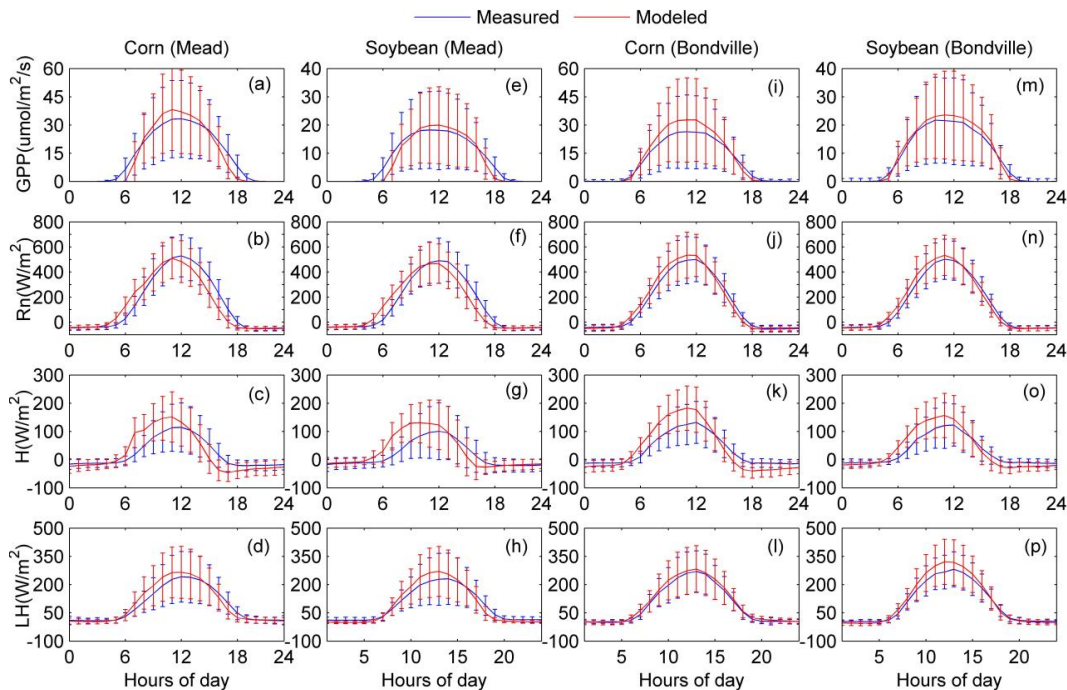
Fig. 1. Measured and model simulated diurnal averaged gross primary productivity (GPP), net radiation (Rn) at the canopy top, sensible heat (H), latent heat (LH) under corn and soybean at Mead and Bondville site over 2001–2004 growing period.
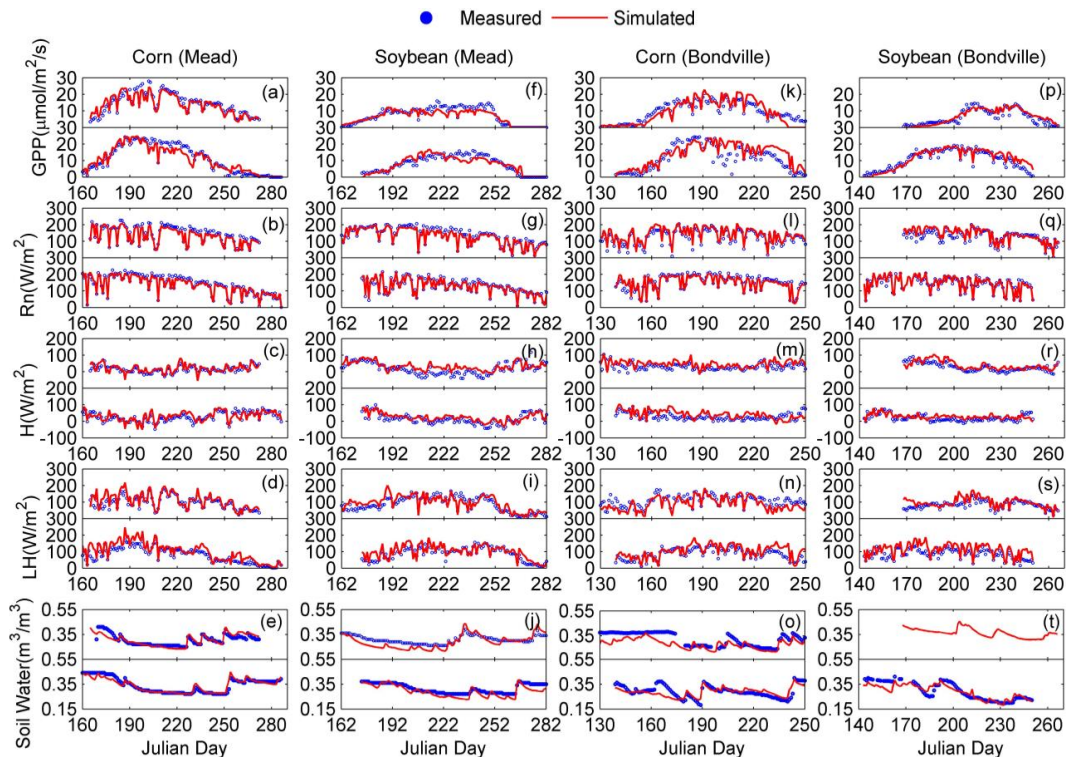
Fig. 2. Measured and model simulated daily mean gross primary productivity (GPP), net radiation (Rn) top of the canopy, sensible heat (*H*), latent heat (LH), and soil water (SW) under corn and soybean rotation at Mead and Bondville over 2001–2004 growing seasons. The top panels are for 2001 and 2002 growing seasons for corn and soybean; whereas the bottom panels are for 2003 and 2004.

Title Page

Abstract | Introduction

Conclusions | References

Tables | Figures

|◄ | ►|

◄ | ►

Back | Close

Full Screen / Esc

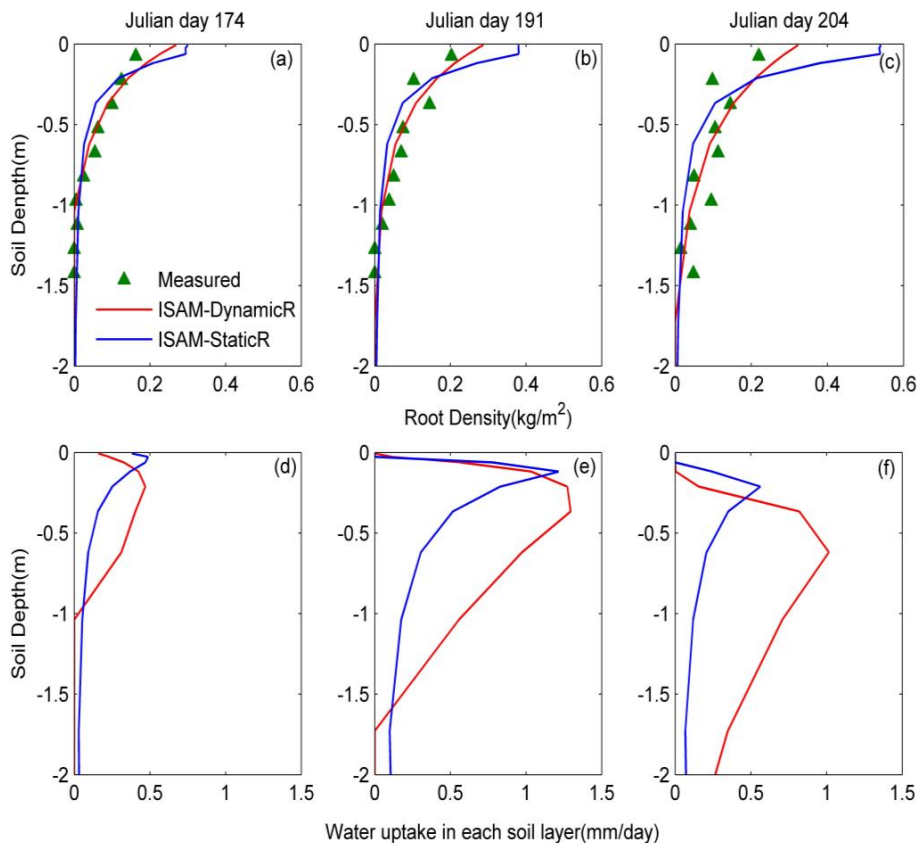Printer-friendly Version

Interactive Discussion

Fig. 3. Comparison of modeled and measured corn root density **(a–c)** and water uptake **(e–f)** profiles (0–2 m) for three different days during the growing season at Mead site. The data and model results for dynamics (ISAM-DynamicR) and Static (ISAM-StatcR) cases are plotted for year 1980.
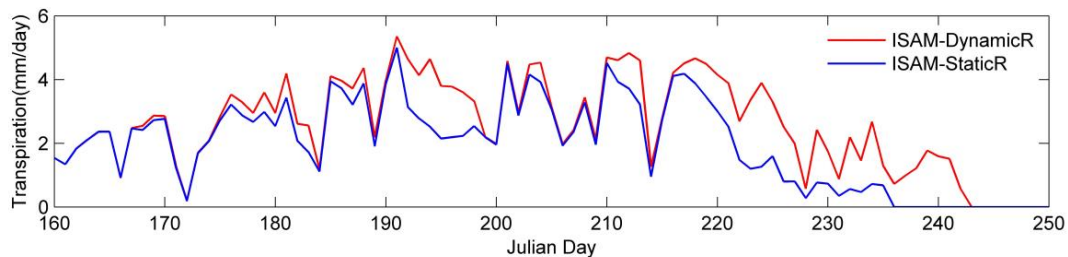
Title Page

Abstract · Introduction

Conclusions · References

Tables · Figures

◀ · ▶

◀ · ▶

Back · Close

Full Screen / Esc

Printer-friendly Version

Interactive Discussion

Fig. 4. Model estimated Daily water uptake for ISAM-DynamicsR and StaticR-ISAMR cases during the 2001 corn growing season at Mead site.
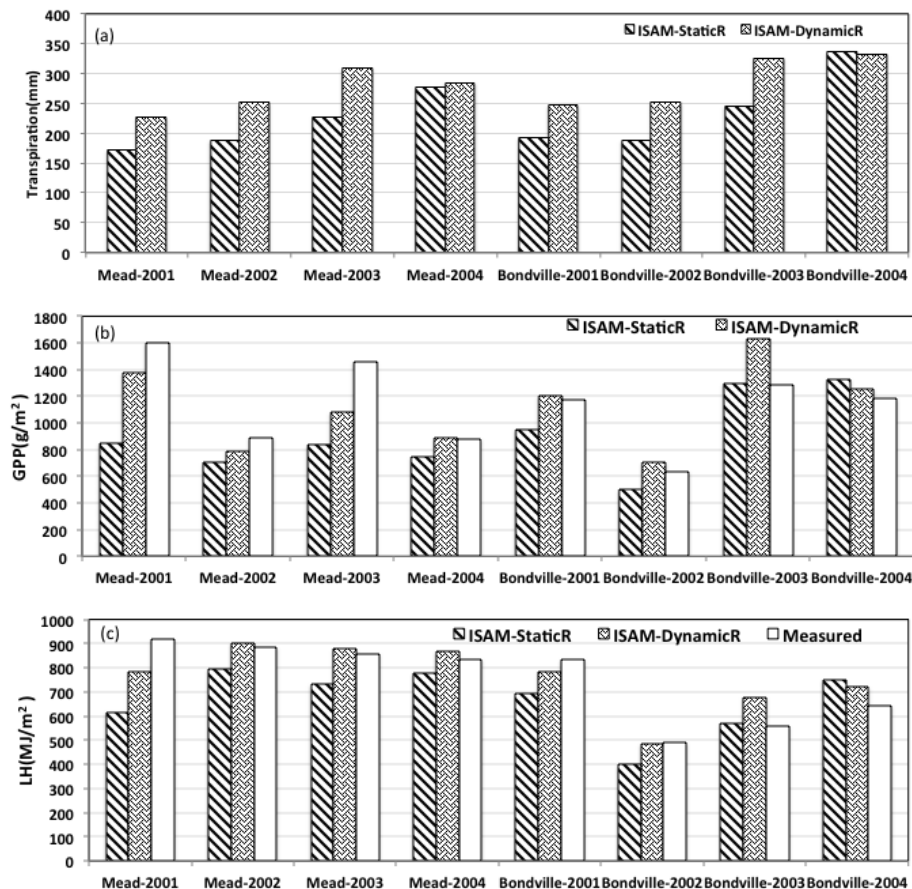
Fig. 5. Measured and simulated total GPP, transpiration and latent heat fluxes (LH) from 2001to 2004 growing season under corn-soybean rotation at Mead and Bondville sites.

Title Page

Abstract | Introduction

Conclusions | References

Tables | Figures

|◄ | ►|

◄ | ►

Back | Close

Full Screen / Esc

Printer-friendly Version

Interactive Discussion